

Silent synapses dictate cocaine memory destabilization and reconsolidation

William J. Wright^{1,6}, Nicholas M. Graziane^{1,2,6}, Peter A. Neumann¹, Peter J. Hamilton³, Hannah M. Cates³, Lauren Fuerst¹, Alexander Spenceley¹, Natalie MacKinnon-Booth¹, Kartik Iyer¹, Yanhua H. Huang¹, Yavin Shaham¹, Oliver M. Schlüter¹, Eric J. Nestler¹ and Yan Dong^{1,4*}

Cocaine-associated memories are persistent, but, on retrieval, become temporarily destabilized and vulnerable to disruptions, followed by reconsolidation. To explore the synaptic underpinnings for these memory dynamics, we studied AMPA receptor (AMPAR)-silent excitatory synapses, which are generated in the nucleus accumbens by cocaine self-administration, and subsequently mature after prolonged withdrawal by recruiting AMPARs, echoing acquisition and consolidation of cocaine memories. We show that, on memory retrieval after prolonged withdrawal, the matured silent synapses become AMPAR-silent again, followed by re-maturation ~6 h later, defining the onset and termination of a destabilization window of cocaine memories. These synaptic dynamics are timed by Rac1, with decreased and increased Rac1 activities opening and closing, respectively, the silent synapse-mediated destabilization window. Preventing silent synapse re-maturation within the destabilization window decreases cue-induced cocaine seeking. Thus, cocaine-generated silent synapses constitute a discrete synaptic ensemble dictating the dynamics of cocaine-associated memories and can be targeted for memory disruption.

Consuming drugs of abuse produces drug-associated memories, which promote subsequent drug seeking and relapse^{1,2}. Similar to other forms of memories³, previously formed and consolidated drug memories can be retrieved on re-exposure to cues associated with earlier drug experience⁴. On retrieval, drug-related memories are transiently destabilized and become susceptible to disruption; the memories are then reconsolidated and become stable again^{5,6}. Without knowing precise neuronal substrates underlying drug memories and their dynamics, aggressive but nonspecific amnestic manipulations, such as protein synthesis inhibition or beta-adrenergic receptor inhibition, within, but not outside of, the destabilization window effectively compromise drug memories and reduce subsequent drug seeking in rodent models^{5–7}. However, nonspecific manipulations with more tolerable regimens fail to demonstrate consistent anti-relapse efficacy in human drug users^{8–10}. These findings highlight the therapeutic potential of using the memory destabilization window for anti-relapse treatments, but also call for the need to identify precise neuronal and molecular substrates encoding the dynamics of drug memories.

Synapses are likely the basic cellular units encoding memory traces. In search of a specific set of synapses encoding cocaine memories, we focused on nucleus accumbens (NAc) medium spiny neurons (MSNs), which are essential in acquiring and maintaining many forms of addiction-related memories, including cue-induced cocaine seeking, a behavioral readout driven by cue-associated cocaine memories². The function of NAc MSNs is driven by excitatory synapses arising from several cortical and subcortical projections, with each input thought to mediate specific responses. Amongst such heterogeneous synapses emerges a unique population, which is generated de novo by cocaine experience,

and is thus cocaine-specific. These synapses are formed within several NAc projections at low levels, but have common cellular features that distinguish them from other synapses. Namely, they are nascent, immature excitatory synapses that contain NMDA receptors (NMDARs) without stable AMPARs, and are thus AMPAR-silent^{11–15}. After generation by cocaine self-administration, these silent synapses mature over time by recruiting calcium-permeable AMPARs (CP-AMPARs), and this maturing and strengthening process results in further enhancement, or incubation, of cue-induced cocaine seeking^{16–18}. These results led to our hypothesis that the functional states of cocaine-generated silent synapses dictate the dynamics of cocaine-associative memories. To test this hypothesis, we examined the role of NAc silent synapses in retrieval-induced destabilization and subsequent reconsolidation of cocaine memories. We trained rats in the cocaine self-administration procedure to establish cue-associative cocaine memories. Cue re-exposure, after prolonged drug withdrawal, induces retrieval and destabilization of cocaine memories. Coincidentally, the matured cocaine-generated synapses become AMPAR-silent and weakened again for ~6 h, and then re-matured and re-strengthened thereafter. These synaptic dynamics, which define the onset and termination of retrieval-induced destabilization of cocaine memories, respectively, were timed by the small GTPase Rac1 and involved bidirectional synaptic trafficking of CP-AMPARs. Rac1- and CP-AMPAR-based manipulations of silent synapse dynamics during, but not outside of, the 6-h destabilization window decreased subsequent cue-induced cocaine seeking. These findings indicate that the functional states of cocaine-generated silent synapses dictate key aspects of cocaine memories, and can be targeted to manipulate cocaine memories and reduce cocaine relapse.

¹Department of Neuroscience, University of Pittsburgh, Pittsburgh, PA, USA. ²Departments of Anesthesiology and Perioperative Medicine and Pharmacology, Penn State College of Medicine, Hershey, PA, USA. ³Nash Family Department of Neuroscience and Friedman Brain Institute, Icahn School of Medicine at Mount Sinai, New York, NY, USA. ⁴Department of Psychiatry, University of Pittsburgh, Pittsburgh, PA, USA. ⁵Behavioral Neuroscience Branch, Intramural Research Program, National Institute on Drug Abuse, National Institutes of Health, Bethesda, MD, USA. ⁶These authors contributed equally: William J. Wright, Nicholas M. Graziane. *e-mail: yandong@pitt.edu

Results

Memory retrieval re-silences cocaine-generated synapses. We trained rats to self-administer cocaine, during which each intravenous infusion was paired with a light cue to form cocaine–cue associations. Consistent with our previous studies^{16–18}, rats acquired cue-associated cocaine memories after 5 d of self-administration, manifested by cue-induced cocaine seeking on withdrawal day 1. This cue-induced cocaine seeking ‘incubated’ during drug abstinence¹⁹ and became greater after 45 d of withdrawal (Fig. 1a–c). Thus, cue-associated cocaine memories are formed during drug self-administration training and strengthened/consolidated during prolonged drug withdrawal.

To assess silent synapses after cocaine memory formation and consolidation, we performed the minimal stimulation assay to estimate the percentage of silent synapses among all sampled synapses in NAc shell (NAcSh) MSNs (Fig. 1d,e). As demonstrated previously^{12,15}, if silent synapses are present in the set of recorded synapses, the failure rate in response to minimal stimulation at +50 mV is lower than that at –70 mV, and based on the differential failure rates, the percentage of silent synapses can be estimated (Fig. 1e) (see Methods). After 1 d of withdrawal from cocaine self-administration, the percentage of silent synapses in NAcSh MSNs was significantly increased (Fig. 1f–h and Supplementary Fig. 1a–c). After prolonged (45 d) withdrawal, the percentage of silent synapses decreased to control levels (Fig. 1h and Supplementary Fig. 1d–g). Our previous studies demonstrate that this decrease is partially due to the maturation and synaptic strengthening process, during which cocaine-generated synapses recruit CP-AMPARs and become unsilenced, contributing to the enhancement of cue-induced cocaine seeking after withdrawal^{16,18}. This maturation is confirmed in our

randomly sampled synapses; application of NASPM (200 μM), a selective CP-AMPAR antagonist, restored the percentage of silent synapses to the high levels observed after 1 d of withdrawal from cocaine self-administration (Fig. 1h and Supplementary Fig. 1h). Thus, cocaine self-administration generates new silent synapses, which subsequently mature after withdrawal via incorporation of CP-AMPARs, potentially contributing to the formation and consolidation of cocaine memories.

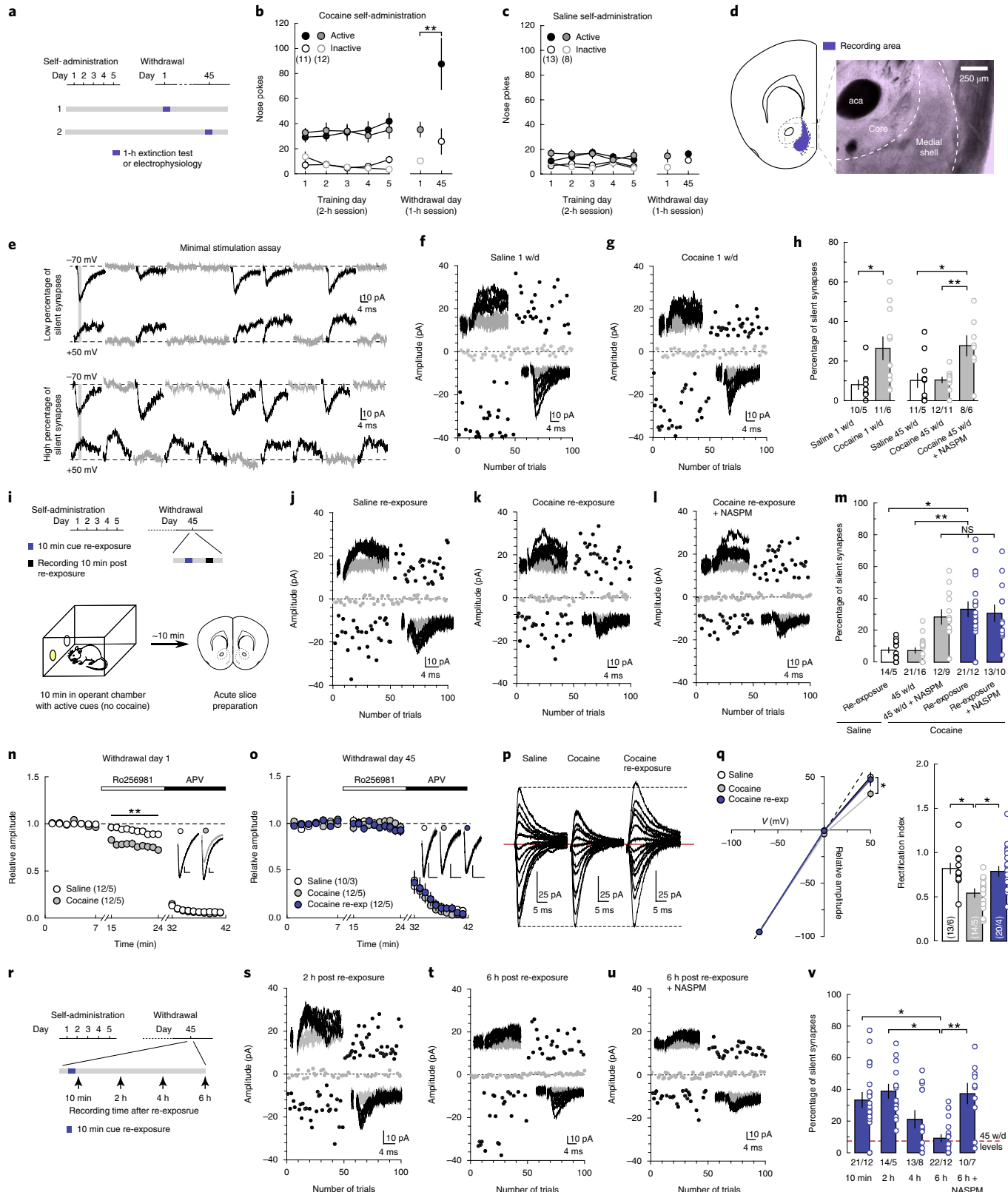
We next examined cue-induced retrieval and destabilization of cocaine memories. After 45 d of withdrawal from cocaine self-administration, we briefly (10 min) re-exposed the rats to cocaine-associated cues through an extinction session in the same operant chambers to reactivate and destabilize cocaine memories⁵. Immediately after cue re-exposure, the rats were analyzed for silent synapses in the NAcSh (Fig. 1i). Cue re-exposure had no effect on the percentage of silent synapses in rats previously trained with saline self-administration, indicating that, without the cocaine–cue pairing, re-exposure to the light cue does not generate new synapses in the NAcSh (Fig. 1j,m and Supplementary Fig. 1i,j). However, the percentage of silent synapses was increased in cocaine-trained rats with cue re-exposure compared with cocaine-trained rats without cue re-exposure (Fig. 1k,m and Supplementary Fig. 1i–q). The magnitude of this cue re-exposure-induced increase in percentage of silent synapses was comparable to the increase induced by CP-AMPAR inhibition in cocaine-trained rats without cue re-exposure (Fig. 1k,m and Supplementary Fig. 1r). Since the cocaine-generated silent synapses mature by recruiting CP-AMPARs, we speculated that cue re-exposure-induced silent synapses are the mature cocaine-generated synapses after losing CP-AMPARs. Consistent with this hypothesis, inhibiting CP-AMPARs did not

Fig. 1 | Memory retrieval re-silences cocaine-generated synapses. **a**, Diagram showing experimental timeline. **b,c**, Summary showing that after cocaine (**b**), but not saline (**c**), self-administration, cue-induced seeking was higher on withdrawal day 45 than withdrawal day 1 (withdrawal day 1, active = 35.08 ± 5.787 , $n=12$; withdrawal day 45, active = 87.13 ± 20.367 , $n=11$; $F_{1,38} = 12.27$, $P = 0.0012$, two-way ANOVA; ** $P < 0.01$, Bonferroni post-test). **d**, Diagram showing the recording area. **e**, Example EPSCs in the minimal stimulation assay, in which failed and successful responses were readily discernable at both –70 mV and +50 mV, and the small versus large failure rate differences between these two holding potentials connote low percentage (top) versus high percentage of silent synapses. **f,g**, EPSCs evoked at –70 mV or +50 mV (insets) over 100 trials from example recordings 1d after saline (**f**) or cocaine (**g**) self-administration. **h**, Summary showing that the percentage of silent synapses was increased on withdrawal day 1 after cocaine self-administration (saline = 5.93 ± 1.44 , $n=5$ animals; cocaine = 24.95 ± 7.13 , $n=6$ animals; $t_0 = 2.38$, $P = 0.04$, two-tail unpaired t-test). On withdrawal day 45, the percentage of silent synapses returned to basal levels, while CP-AMPAR inhibition restored the high percentage of silent synapses (saline = 11.71 ± 5.35 , $n=5$ animals; cocaine = 10.53 ± 1.49 , $n=11$ animals; cocaine NASPM = 28.37 ± 4.68 , $n=6$ animals; $F_{2,19} = 8.61$, $P = 0.0022$, one-way ANOVA; * $P < 0.05$, ** $P < 0.01$, Bonferroni post-test). **i**, Diagram showing experimental timeline. **j–l**, EPSCs evoked at –70 mV or +50 mV by minimal stimulation (insets) over 100 trials from example recordings after cue re-exposure from saline- (**j**) and cocaine-trained rats (**k**) in the absence or presence (**l**) of NASPM. **m**, Summary showing that cue re-exposure increased the percentage of silent synapses in cocaine-trained, but not saline-trained, rats on withdrawal day 45, and the effects of NASPM (saline re-exp = 7.74 ± 1.89 , $n=5$ animals; cocaine 45 w/d = 8.01 ± 1.89 , $n=16$ animals; cocaine 45 w/d NASPM = 31.31 ± 5.22 , $n=9$ animals; cocaine re-exp = 32.89 ± 5.41 , $n=12$ animals; cocaine re-exp NASPM = 29.74 ± 3.85 , $n=10$; $F_{4,47} = 10.11$, $P < 0.0001$, one-way ANOVA; NS > 0.05, * $P < 0.05$, ** $P < 0.01$, Bonferroni post-test). **n**, Summary showing increased sensitivity to Ro256981 of NMDAR EPSCs in rats 1d after cocaine self-administration (saline = 0.91 ± 0.03 at 24 min, $n=5$ animals; cocaine = 0.74 ± 0.03 at 24 min, $n=5$ animals; $F_{26,104} = 7.66$, $P < 0.0001$, two-way repeated-measures (RM) ANOVA; ** $P < 0.01$, Bonferroni post-test). Subsequent application of APV (50 μM) confirmed that currents were mediated by NMDARs. Inset: example NMDAR EPSCs before and during Ro256981 application. **o**, Summary showing that cue re-exposure did not affect the Ro256981 sensitivity of NMDAR EPSCs in NAcSh MSNs (saline = 0.93 ± 0.03 at 24 min, $n=3$ animals; cocaine = 0.92 ± 0.06 at 24 min, $n=5$ animals; cocaine re-exp = 0.93 ± 0.05 at 24 min, $n=5$; $F_{52,260} = 0.50$, $P = 0.9984$, two-way RM ANOVA). **p**, Example AMPAR EPSCs evoked from holding potentials of –70 mV to +50 mV with 10-mV increments. **q**, Left, I–V curves of AMPAR EPSCs showing rectification in cocaine-trained rats on withdrawal day 45, and the rectification was abolished by cue re-exposure (saline = 52.51 ± 5.68 , $n=6$ animals; cocaine = 29.98 ± 3.17 , $n=5$ animals; cocaine re-exp = 43.93 ± 6.01 , $n=4$ animals; $F_{4,33} = 4.15$, $P = 0.0078$, two-way ANOVA; * $P < 0.05$, Bonferroni post-test). EPSC amplitudes at –70 mV were used to normalize EPSCs at other membrane potentials. Right: summary showing that on withdrawal day 45, the decreased rectification index in cocaine-trained rats was abolished by cue re-exposure (saline = 0.79 ± 0.051 , $n=6$ animals; cocaine = 0.54 ± 0.041 , $n=5$ animals; cocaine re-exp = 0.79 ± 0.057 , $n=4$ animals; $F_{2,12} = 8.06$, $P = 0.006$, one-way ANOVA; * $P < 0.05$, Bonferroni post-test). The 10-min data were taken from **m**. See Supplementary Table 1 for exact P values for all comparisons made during post hoc tests. Data presented as mean ± s.e.m. aca, anterior commissure; NS, not significant; re-exp, re-exposure; w/d, withdrawal day.

further increase the percentage of silent synapses in cocaine-trained rats after cue re-exposure (Fig. 1k–m).

While cue re-exposure did not generate new silent synapses in saline-trained rats (Fig. 1j,m and Supplementary Fig. 1i,j), it may do so in cocaine-trained rats, similar to what occurs 1 d after cocaine self-administration. Generation of new silent synapses after cocaine

experience involves synaptic insertion of GluN2B-containing NMDARs^{12,20}. This was confirmed in our current experiments, in which NMDAR-mediated excitatory postsynaptic currents (EPSCs) in NAcSh MSNs exhibited increased sensitivity to the GluN2B-selective antagonist Ro256981 (200 nM) after 1 d of withdrawal from cocaine self-administration (Fig. 1n and Supplementary Fig. 2a,b).



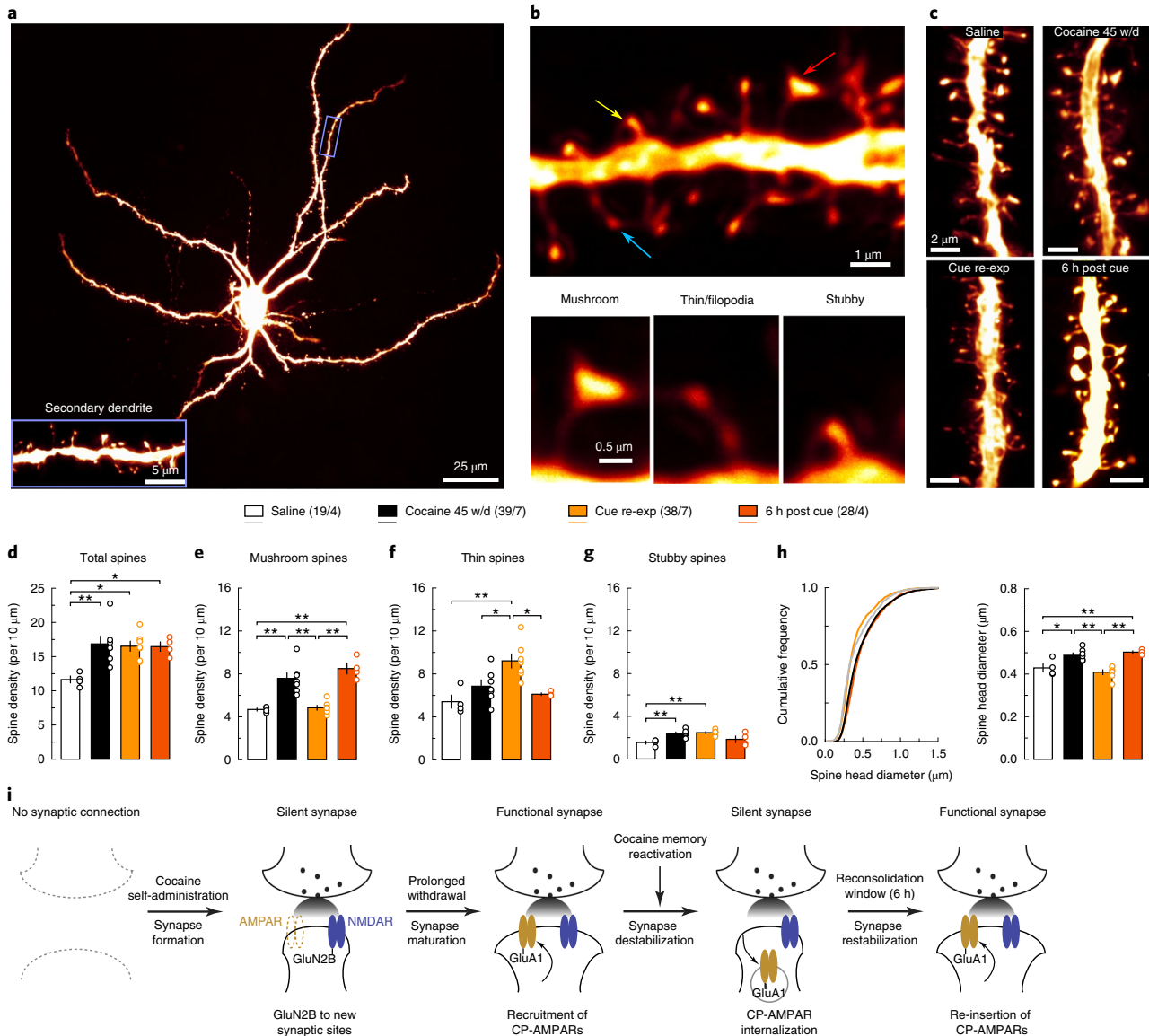


Fig. 2 | Spine morphology correlate with memory destabilization and reconsolidation. **a**, Example image showing an NAcSh MSN filled with Alexa Fluor 594 dye, and a magnified secondary dendrite (inset). Replicates for each group are presented in **d–h** with n values. **b**, Example spiny dendrites (top) and three subtypes of spines (bottom) whose dendritic locations are indicated by arrows; mushroom (red), thin (blue) and stubby (yellow). Replicates for each group are presented in **d–h** with n values. **c**, Example NAcSh dendrites from saline-trained rats with cue re-exposure (top left), cocaine-trained rats without (top right), 10 min after (bottom left) and 6 h after (bottom right) cue re-exposure on withdrawal day 45. Replicates for each group are presented in **d–h** with n values. **d**, Summary showing that the density of total spines was increased after 45 d of withdrawal from cocaine compared with saline controls, and this increase was not altered by cue re-exposure and reconsolidation (saline = 11.66 ± 0.49 , $n = 4$ animals; cocaine 45 w/d = 16.86 ± 1.12 , $n = 7$ animals; cocaine re-exp = 16.53 ± 0.716 , $n = 7$ animals; cocaine 6 h post = 16.46 ± 0.665 , $n = 4$ animals; $F_{3,18} = 5.98$, $P = 0.0051$, one-way ANOVA; * $P < 0.05$, ** $P < 0.01$, Bonferroni post-test). **e**, Summary showing that the density of mushroom-like spines was increased after 45 d of withdrawal from cocaine compared with saline controls. Cue re-exposure decreased mushroom-like spine density to saline levels, while this cue re-exposure-induced effect disappeared 6 h later (saline = 4.68 ± 0.129 , $n = 4$; cocaine 45 w/d = 7.57 ± 0.531 , $n = 7$; cocaine re-exp = 4.84 ± 0.215 , $n = 7$; cocaine 6 h post = 8.50 ± 0.493 , $n = 4$; $F_{3,18} = 19.86$, $P < 0.0001$, one-way ANOVA; ** $P < 0.01$, Bonferroni post-test). **f**, Summary showing that the density of thin spines was increased by cue re-exposure in cocaine-trained rats compared with saline-trained rats or cocaine rats without re-exposure. Density of thin spines normalized 6 h after re-exposure (saline = 5.43 ± 0.598 , $n = 4$ animals; cocaine 45 w/d = 6.86 ± 0.568 , $n = 7$ animals; cocaine re-exp = 9.21 ± 0.643 , $n = 7$ animals; cocaine 6 h post = 6.12 ± 0.107 , $n = 4$ animals; $F_{3,18} = 7.89$, $P = 0.0014$, one-way ANOVA; * $P < 0.05$, ** $P < 0.01$, Bonferroni post-test). **g**, Summary showing that the density of stubby spines was increased in cocaine-trained rats with or without cue re-exposure, compared with saline-trained rats (saline = 1.56 ± 0.142 , $n = 4$ animals; cocaine 45 w/d = 2.41 ± 0.115 , $n = 7$ animals; cocaine re-exposure = 2.47 ± 0.09 , $n = 7$ animals; cocaine 6 h post = 1.85 ± 0.295 , $n = 4$ animals; $F_{3,18} = 8.28$, $P = 0.001$, one-way ANOVA; ** $P < 0.01$, Bonferroni post-test). **h**, Summary of cumulative frequency (left) and mean values (right) showing an increase in the overall spine head diameter in cocaine-trained rats compared with saline controls. Spine head diameter in cocaine-trained rats decreased to saline levels after cue re-exposure, which normalized 6 h after re-exposure (saline = 0.429 ± 0.019 , $n = 4$ animals; cocaine 45 w/d = 0.488 ± 0.011 , $n = 7$ animals; cocaine re-exp = 0.401 ± 0.011 , $n = 7$ animals; cocaine 6 h post = 0.503 ± 0.005 , $n = 4$ animals; $F_{3,18} = 14.67$, $P < 0.0001$, one-way ANOVA; * $P < 0.05$, ** $P < 0.01$, Bonferroni post-test). **i**, Schematic illustration depicting the hypothesized dynamics of cocaine-generated silent synapses during acquisition, consolidation, destabilization and reconsolidation of cocaine-associated memories. See Supplementary Table 1 for exact P values for all comparisons made during post hoc tests. Data are presented as mean \pm s.e.m.

On withdrawal day 45, the sensitivity of NMDAR EPSCs to Ro256981 declined to low levels (Fig. 1o and Supplementary Fig. 2c,d), suggesting that GluN2B NMDARs had been replaced with other NMDAR subtypes, which is consistent with the maturation of nascent synapses²¹. Importantly, cue re-exposure did not alter the low sensitivity of NMDARs to Ro256981 in cocaine-trained rats (Fig. 1o), indicating that cue re-exposure did not trigger GluN2B-mediated de novo generation of silent synapses.

While GluN2B NMDARs were not changed by cue re-exposure in cocaine-trained rats, we detected internalization of CP-AMPARs. CP-AMPARs conduct minimal current at depolarized potentials²², and can thus be detected by an increased inward rectification. In saline-trained rats, very low levels of CP-AMPARs are expressed at excitatory synapses on NAcSh MSNs, reflected as a linear current-voltage (*I*-*V*) relationship of AMPAR EPSCs (Fig. 1p,q). After 45 d of withdrawal from cocaine, AMPAR EPSCs become inwardly rectifying (Fig. 1p,q and Supplementary Fig. 2e,f), indicative of CP-AMPAR incorporation to cocaine-generated synapses, as observed previously^{16,18,23}. Cue re-exposure, however, normalized this rectification (Fig. 1p,q), suggesting removal of CP-AMPARs. Taken together, these results support a scenario of CP-AMPAR internalization-mediated re-silencing of matured silent synapses.

Retrieval-induced memory destabilization lasts ~6 h before reconsolidation^{4,24}. The dynamics of NAcSh silent synapses exhibited similar time course after cue re-exposure (Fig. 1r). Specifically, the percentage of silent synapses remained high 2 or 4 h after cue re-exposure, but returned to low levels after 6 h (Fig. 1s–v and Supplementary Fig. 1m–s). At the 6-h time point, inhibition of CP-AMPARs by NASPM restored the high percentage of silent synapses (Fig. 1q,v), suggesting that the cue-re-silenced synapses re-mature by re-insertion of CP-AMPARs. Thus, the already matured silent synapses are re-silenced and weakened via internalization of CP-AMPARs on cue re-exposure, and then re-matured 6 h later. Thus, re-silencing and subsequent re-maturation of silent synapses follow the general time course of retrieval-induced destabilization and reconsolidation of cocaine memories.

The morphology of dendritic spines is correlated with the maturational state of glutamatergic synapses²⁵. In NAcSh slices, we filled MSNs with Alexa 594 dye and imaged their secondary dendrites, which receive dense glutamatergic inputs (Fig. 2a). NAcSh dendritic spines can be categorized into at least four subtypes: (1) mushroom-like spines, (2) long-thin spines, (3) filopodia-like spines and (4) stubby spines (Fig. 2b) (see Methods)²⁰. It is thought that mushroom-like spines represent mature synapses enriched in AMPARs, while long-thin and filopodia-like spines are relatively immature synapses with few or no AMPARs²⁵. This relationship is supported by our previous studies examining cocaine-induced silent synapses in the NAcSh²⁰. Due to their morphological and functional similarity, we combined long-thin and filopodia-like spines for data interpretation.

Similar to previous studies²⁰, on withdrawal day 1 after cocaine self-administration, the density of total spines was increased compared with saline-trained rats (Supplementary Fig. 3a,b). This increase was primarily attributable to an increase in thin spines (Supplementary Fig. 3c–g) that likely correspond to newly generated silent synapses. We also observed a small increase in the density of stubby spines (Supplementary Fig. 3e), but given their low basal density and small contribution (~4%) to the total spine density change, their role in generation of silent synapses was considered to be minimal. On withdrawal day 45, the total spine density remained higher in cocaine-trained rats compared with saline-trained rats (Fig. 2c,d and Supplementary Fig. 3i–l). However, the density of thin spines in cocaine-trained rats returned to levels comparable to saline-trained rats (Fig. 2f). In contrast, the density of mushroom-like spines was increased in cocaine-trained rats (Fig. 2e). The density of stubby spines was also slightly higher in

cocaine-trained rats compared with saline-trained rats (Fig. 2g). These spine patterns are consistent with the notion that cocaine-generated silent synapses mature and stabilize by recruiting AMPARs after 45 d of withdrawal.

After 45 d of withdrawal from cocaine self-administration, cue re-exposure did not alter the density of total spines, such that they remained high, comparable to cocaine-trained rats without cue re-exposure (Fig. 2c,d). However, under these conditions, the density of mushroom-like spines decreased to lower levels, similar to saline-trained rats (Fig. 2c,e). This decrease coincided with an increase in the density of thin spines (Fig. 2c,f). Stubby spines were unaffected by cue re-exposure (Fig. 2c,g). The simultaneous downshift of mushroom-like spines and upshift of thin spines suggest that some mature synapses return to a weakened, immature state, consistent with the notion that matured silent synapses are re-silenced after cue re-exposure. Furthermore, 6 h after cue re-exposure, the densities of mushroom-like and thin spines returned to levels similar to the cocaine-trained rats without cue re-exposure, with no change in the density of total spines (Fig. 2d–g). Thus, the weakened spines re-mature by the end of the destabilization window, corresponding to re-maturation of silent synapses and memory reconsolidation.

The diameter of spine heads can be used as an additional measure of synaptic strength complementary to the above morphological classification²⁶. After 45 d of withdrawal from cocaine self-administration, the mean diameter of spine heads was increased compared with saline-trained rats (Fig. 2h). Following cue re-exposure, the mean diameter of spine heads decreased to saline control levels (Fig. 2h), suggesting synaptic weakening or re-silencing. However, 6 h after cue re-exposure, the mean diameter of spine heads returned to the level of cocaine-trained rats without cue re-exposure (Fig. 2h), suggesting re-strengthening or re-maturation of synapses.

Based on the above results, we hypothesized that the states of NAc silent synapses, including their generation, maturation, re-silencing and re-maturation, contribute to the formation, consolidation, retrieval-induced destabilization and reconsolidation of cocaine memories, respectively (Fig. 2i). We tested this hypothesis in the experiments described below.

Synapse re-silencing destabilizes cocaine memories. To determine the role of silent synapse dynamics in destabilization and subsequent reconsolidation of cocaine memories, we adopted a manipulation to prevent re-maturation of silent synapses after cue re-exposure by preventing re-insertion of CP-AMPARs (Fig. 3a). Specifically, the small peptide TGL can bind to the C terminus of GluA1 subunits to disrupt synaptic insertion of GluA1-containing AMPARs, which are the predominant population of cocaine-induced CP-AMPARs^{2,27}. We conjugated TGL and its mutant control peptide AGL with a TAT sequence to allow intracellular delivery *in vivo*. To verify the efficacy of this peptide, we induced a subtype of long-term potentiation (LTP) in the hippocampal CA1 (Supplementary Fig. 4a), whose expression primarily relies on synaptic insertion of GluA1 AMPARs^{28,29}. Preincubation of hippocampal slices with TGL, but not AGL, prevented this GluA1 AMPAR-dependent LTP (Supplementary Fig. 4a), validating this peptide-based approach.

We infused TGL or AGL (30 μM per side) into the NAcSh of rats ~2 h after cue re-exposure on withdrawal day 45 (Fig. 3b), conditions under which silent synapses re-emerged in cocaine-trained rats (Fig. 1v). We then assessed percentage of silent synapses 6 h after cue re-exposure, the time point at which the synapses re-silenced by cue re-exposure have normally re-matured (Fig. 1v). Infusion of either peptide did not alter the percentage of silent synapses in saline-trained rats (Fig. 3c,f and Supplementary Fig. 4b,d,e), suggesting that these peptides do not influence silent synapses at baseline. Cocaine-trained rats with NAcSh AGL exhibited low percentage of silent synapses, which was increased by NASPM, indicating the expected re-maturation of silent synapses (Fig. 3d,f and Supplementary Fig. 4c,d,f).

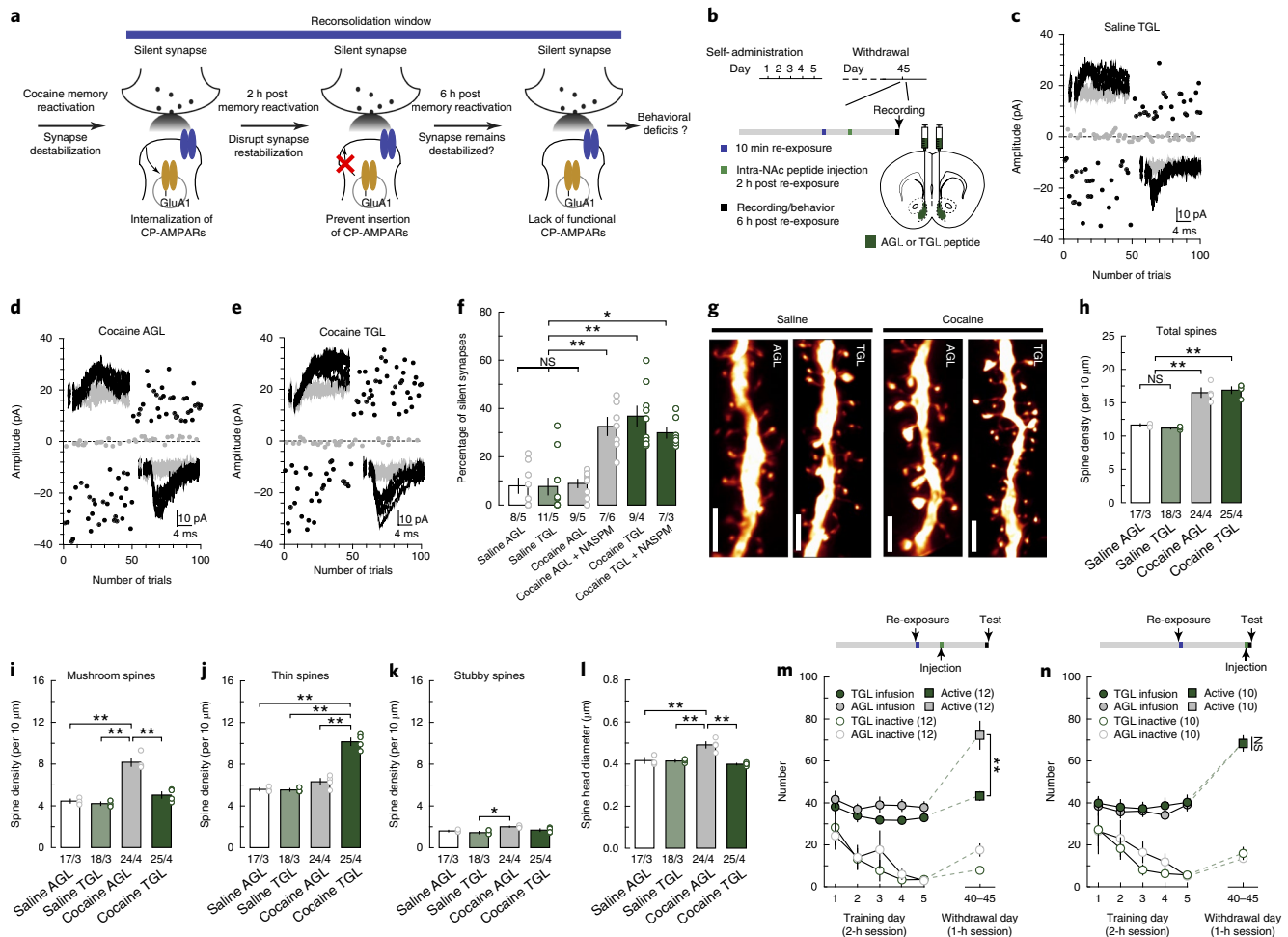


Fig. 3 | Synapse re-silencing destabilizes cocaine memories. **a**, Diagram illustrating the hypothesis that preventing CP-AMPAR re-insertion during the reconsolidation window locks cocaine-generated synapses in the silent state and compromises cue-induced cocaine seeking. **b**, Diagram showing experimental timeline. **c-d,e**, Example EPSCs evoked at -70 mV and $+50\text{ mV}$ by minimal stimulation (insets) over 100 trials from saline- (**c**) or cocaine-trained (**d**) rats with NAcSh TGL infusion and the effects of NASPM (**e**). **f**, Summary showing that while intra-NAcSh TGL or AGL did not affect the percentage of silent synapses in saline-trained rats, intra-NAcSh TGL, but not AGL, maintained the cue re-exposure-induced high percentage of silent synapses in cocaine-trained rats beyond the presumable 6-h destabilization window, and CP-AMPAR inhibition by NASPM did not further affect the percentage of silent synapses (saline AGL = 6.40 ± 3.68 , $n=5$ animals; saline TGL = 7.06 ± 3.07 , $n=5$ animals; cocaine AGL = 9.70 ± 1.05 , $n=5$ animals; cocaine AGL NASPM = 33.76 ± 3.71 , $n=6$ animals; cocaine TGL = 37.10 ± 3.71 , $n=4$ animals; cocaine TGL NASPM = 29.70 ± 3.08 , $n=3$ animals; $F_{5,22} = 14.85$, $P < 0.0001$, one-way ANOVA; NS > 0.05, $*P < 0.05$, $**P < 0.01$, Bonferroni post-test). **g**, Example NAcSh dendrites from saline-trained rats and cocaine-trained rats with AGL and TGL infusions. Scale bar, $2.5\text{ }\mu\text{m}$. **h**, Summary showing that the density of total spines was increased in cocaine-trained rats with either AGL or TGL compared with saline-trained rats (saline AGL = 11.66 ± 0.171 , $n=3$ animals; saline TGL = 11.20 ± 0.146 , $n=3$ animals; cocaine AGL = 16.52 ± 0.69 , $n=4$ animals; cocaine TGL = 16.89 ± 0.488 , $n=4$ animals; $F_{3,10} = 36.01$, $P < 0.0001$, one-way ANOVA; NS > 0.05, $**P < 0.01$, Bonferroni post-test). **i**, Summary showing that the density of mushroom-like spines was increased in cocaine-trained rats with AGL compared with saline-trained rats, while TGL treatment normalized mushroom-like spine density to saline levels (saline AGL = 4.46 ± 0.19 , $n=3$ animals; saline TGL = 4.23 ± 0.163 , $n=3$ animals; cocaine AGL = 8.18 ± 0.383 , $n=4$ animals; cocaine TGL = 5.04 ± 0.302 , $n=4$ animals; $F_{3,10} = 38.59$, $P < 0.0001$, one-way ANOVA; $**P < 0.01$, Bonferroni post-test). **j**, Summary showing that the density of thin spines was significantly increased in cocaine-trained TGL rats compared with cocaine-trained AGL rats or saline-trained rats (saline AGL = 5.60 ± 0.148 , $n=3$ animals; saline TGL = 5.54 ± 0.132 , $n=3$ animals; cocaine AGL = 6.33 ± 0.309 , $n=4$ animals; cocaine TGL = 10.16 ± 0.363 , $n=4$ animals; $F_{3,10} = 60.80$, $P < 0.0001$, one-way ANOVA; $**P < 0.01$, Bonferroni post-test). **k**, Summary showing densities of stubby spines in saline- and cocaine-trained rats with AGL or TGL treatment (saline AGL = 1.60 ± 0.076 , $n=3$ animals; saline TGL = 1.45 ± 0.117 , $n=3$ animals; cocaine AGL = 2.01 ± 0.051 , $n=4$ animals; cocaine TGL = 1.69 ± 0.118 , $n=4$ animals; $F_{3,10} = 6.32$, $P = 0.0112$, one-way ANOVA; $*P < 0.05$, Bonferroni post-test). **l**, Summary showing that the mean spine head diameter was increased in cocaine-trained AGL rats compared with saline-trained rats, while TGL treatment normalized this increase to saline control levels (saline AGL = 0.417 ± 0.013 , $n=3$ animals; saline TGL = 0.415 ± 0.005 , $n=3$ animals; cocaine AGL = 0.492 ± 0.015 , $n=4$ animals; cocaine TGL = 0.400 ± 0.004 , $n=4$ animals; $F_{3,10} = 16.17$, $P = 0.0004$, one-way ANOVA; $**P < 0.01$, Bonferroni post-test). **m**, Summary showing that intra-NAcSh infusion of TGL, but not AGL, at 2 h after cue re-exposure decreased cue-induced cocaine seeking in cocaine-trained rats, measured 6 h after cue re-exposure (AGL active = 72.25 ± 6.68 , $n=12$ animals; TGL active = 43.25 ± 2.07 , $n=12$ animals; AGL inactive = 17.58 ± 2.90 , $n=12$ animals; TGL inactive = 7.92 ± 1.34 , $n=12$ animals; $F_{1,22} = 12.26$, $P = 0.002$, RM two-way ANOVA, withdrawal day 45 peptide × lever interaction; $**P < 0.01$, Bonferroni post-test). **n**, Summary showing that rats with intra-NAcSh infusion of TGL 6 h after cue re-exposure exhibited similar cue-induced cocaine seeking as AGL rats measured 6.5 h after cue re-exposure (AGL active = 68.20 ± 2.87 , $n=10$ animals; TGL active = 68.20 ± 3.74 , $n=10$ animals; AGL inactive = 13.30 ± 1.69 , $n=10$ animals; TGL inactive = 15.70 ± 2.94 , $n=10$ animals; $F_{1,18} = 0.23$, $P = 0.64$, RM two-way ANOVA, withdrawal day 45 peptide × lever interaction). See Supplementary Table 1 for exact P values for all comparisons made during post hoc tests. Data are presented as mean \pm s.e.m.

In contrast, TGL rats exhibited persistently high percentage of silent synapses, and application of NASPM did not further change this percentage (Fig. 3e,f and Supplementary Fig. 4g). Thus, preventing synaptic insertion of GluA1 AMPARs prevents re-maturation of the re-silenced synapses after cue re-exposure, and locks cocaine-generated synapses in the destabilized state.

Our subsequent results show that, when administered within the destabilization window, TGL also prevented weakened spines from re-maturation (Fig. 3b). Specifically, infusion of TGL 2 h after cue re-exposure did not change the densities of any spine subtypes in saline-trained rats (Fig. 3g-k and Supplementary Fig. 4h-j). However, after 45 d of withdrawal from cocaine, the cue re-exposure-induced upshift of thin spines and downshift of mushroom-like spines, which would otherwise return to the pre-re-exposure levels 6 h later (Fig. 2), were maintained in TGL rats (Fig. 3g-j). Thus, the spines that were weakened by cue re-exposure in cocaine-trained rats (Fig. 2) were effectively locked in their weakened state by TGL-mediated blockade of GluA1 AMPAR trafficking. Consistently, the mean diameter of spine heads in cocaine-trained TGL rats was similar to saline-trained rats, and lower than cocaine-trained AGL rats (Fig. 3l). Meanwhile, cocaine-trained rats with either AGL or TGL infusion exhibited higher densities of total spines compared with saline-trained rats, and AGL did not prevent re-maturation of cue re-exposure-induced thin spines (Fig. 3h-j). Furthermore, stubby spines were largely insensitive to TGL (Fig. 3k).

If re-silencing and re-maturation of cocaine-generated synapses underlie the destabilization and reconsolidation of cocaine memories, preventing their re-maturation should disrupt reconsolidation and decrease the rats' responses to cocaine cues. To test this idea, we treated cocaine-trained rats using the same peptide procedure (Fig. 3b), and measured cocaine seeking 6 h after cue re-exposure, a time point at which cocaine seeking was robust in cocaine-trained rats with no peptide infusion (Supplementary Fig. 5a-c). Infusion

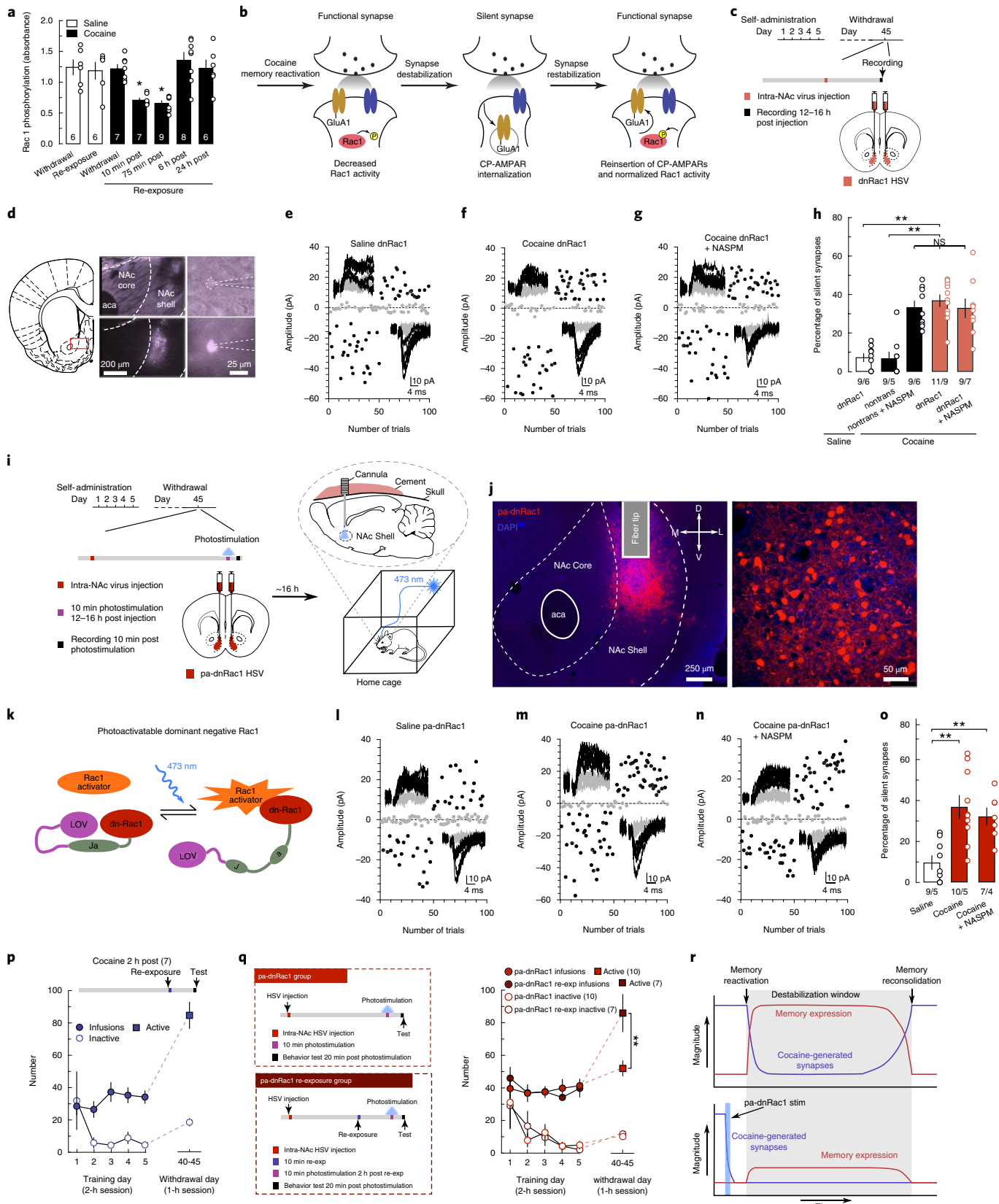
of either AGL or TGL did not affect operant responding in saline-trained rats (Supplementary Fig. 5d,e,g,h), indicating minimal off-target effects of these peptides. However, cocaine-trained TGL rats exhibited decreased cocaine seeking compared with AGL rats when tested 6 h after cue re-exposure, suggesting that preventing re-maturation of cocaine-generated silent synapses once they are re-silenced during the destabilization window compromises reconsolidation of cocaine-cue memories (Fig. 3m and Supplementary Fig. 5i). Note that during the 10-min cue re-exposure, AGL and TGL rats exhibited similar levels of cocaine seeking, indicating similar memory reactivation in these rats before peptide administration (Supplementary Fig. 5f). Importantly, when peptides were infused 6 h after cue re-exposure, a time point outside of the hypothesized destabilization window, cocaine-trained TGL rats exhibited similarly high levels of cocaine seeking as in cocaine-trained AGL rats, suggesting that once silent synapses have re-matured, cocaine memories become resistant to TGL manipulations (Fig. 3n and Supplementary Fig. 5f,j). These results reveal a causal link of the functional dynamics of cocaine-generated synapses to the destabilization and reconsolidation of cocaine memories.

Decreased Rac1 activity primes cue-induced synaptic re-silencing. To explore the molecular mechanisms that switch on and off silent synapse-mediated destabilization of cocaine memories, we focused on Rac1, a small GTPase, whose active forms are enriched in mature synapses to maintain synaptic stability through LIMK-cofilin-mediated regulation of actin cytoskeleton^{30,31}. Using enzyme-linked immunosorbent assay (ELISA), we observed that after cue re-exposure on withdrawal day 45, levels of active Rac1 (Rac1-GTP) in the NAcSh were decreased transiently in cocaine-trained rats, and then returned to normal levels 6 h later (Fig. 4a). As controls, cue re-exposure did not affect levels of active Rac1 in saline-trained rats (Fig. 4a).

Fig. 4 | Decreased Rac1 activity primes cue-induced synaptic re-silencing. **a**, Summarized ELISA results showing transiently decreased levels of active Rac1 in NAcSh on cue re-exposure in cocaine-trained but not saline-trained rats (saline withdrawal = 1.24 ± 0.122 , $n = 6$ animals; saline re-exp = 1.19 ± 0.136 , $n = 6$ animals; cocaine withdrawal = 1.23 ± 0.071 , $n = 7$ animals; cocaine 10 min = 0.708 ± 0.033 , $n = 7$ animals; cocaine 75 min = 0.658 ± 0.041 , $n = 9$ animals; cocaine 6 h = 1.36 ± 0.125 , $n = 8$ animals; cocaine 24 h = 1.23 ± 0.136 , $n = 6$ animals; $P < 0.0001$, one-way ANOVA; * $P < 0.05$, Bonferroni post-test). **b**, Diagram illustrating the hypothesis that the transient downregulation of active Rac1 triggers re-silencing of the already matured silent synapses in cocaine-trained rats. **c**, Diagram showing the timeline for experiments involving intra-NAcSh expression of dnRac1. **d**, Example images showing dnRac1-expressing NAcSh MSNs during recordings. **e-g**, EPSCs evoked at -70 mV and $+50$ mV during the minimal stimulation assay (insets) over 100 trials from example dnRac1-expressing MSNs in saline- (**e**) and cocaine-trained rats (**f**), and the effects of NASPM (**g**). **h**, Summary showing that expressing dnRac1 in NAcSh MSNs increased the percentage of silent synapses selectively in cocaine-trained rats on withdrawal day 45 and that CP-AMPAR inhibition did not further increase this percentage (saline dnRac1 = 7.32 ± 2.73 , $n = 6$ animals; cocaine nontrans = 6.32 ± 2.59 , $n = 5$ animals; cocaine nontrans NASPM = 33.97 ± 4.14 , $n = 6$ animals; cocaine dnRac1 = 36.47 ± 3.46 , $n = 9$ animals; cocaine dnRac1 NASPM = 31.67 ± 4.83 , $n = 7$ animals; $F_{2,28} = 14.46$, $P < 0.0001$, one-way ANOVA; ** $P < 0.01$, Bonferroni post-test). **i**, Diagrams showing the experimental design, in which NAcSh pa-dnRac1 was photoactivated for 10 min while rats remained in their home cage. **j**, Example images of an NAcSh slice (left) and MSNs (right) showing HSV-mediated expression of pa-dnRac1. All animals used in **o** and **q** ($n = 26$ animals) had pa-dnRac1 expression localized within the NAcSh. **k**, Diagram illustrating the design concept of pa-dnRac1. **l-n**, EPSCs evoked at -70 mV and $+50$ mV during the minimal stimulation assay (insets) over 100 trials from example pa-dnRac1-expressing MSNs in saline- (**l**) and cocaine-trained rats (**m**), and the effects of NASPM (**n**). **o**, Summary showing that stimulating pa-dnRac1 on withdrawal day 45 did not affect the percentage of silent synapses in saline-trained rats, but increased the percentage of silent synapses in cocaine-trained rats, and this increase was not affected by NASPM (saline = 9.08 ± 1.70 , $n = 5$ animals; cocaine = 35.91 ± 4.89 , $n = 5$ animals; cocaine NASPM = 33.07 ± 4.21 , $n = 4$ animals; $F_{2,11} = 15.56$, $P = 0.0006$, one-way ANOVA; ** $P < 0.01$, Bonferroni post-test). **p**, Summary showing that the nose poke responding remained at high levels in cocaine-trained rats when tested 2 h after cue re-exposure (cocaine 2 h post = 84.86 ± 8.08 , $n = 7$ animals). **q**, Left: diagrams showing the experimental timeline for cocaine-trained rats that received stimulation of pa-dnRac1 without (top) and with (bottom) previous cue re-exposure. Right: summary showing that rats that received pa-dnRac1 stimulation without previous cue re-exposure exhibited decreased cue-induced cocaine seeking compared with rats with previous (2 h before) cue re-exposure (pa-dnRac1 active = 52.00 ± 4.54 , $n = 10$ animals; pa-dnRac1 re-exp active = 85.71 ± 11.23 , $n = 7$ animals; pa-dnRac1 inactive = 10.50 ± 1.17 , $n = 10$ animals; pa-dnRac1 re-exp inactive = 12.14 ± 2.01 , $n = 7$ animals; $F_{1,15} = 9.17$, $P = 0.0085$, RM two-way ANOVA, withdrawal day 45 lever \times group interaction; ** $P < 0.01$, Bonferroni post-test). **r**, Hypothetical diagrams illustrating the dissociation between the functional state of cocaine-generated synapses and the behavioral expression (seeking) following reactivation of cocaine memories. Top: after cue re-exposure-induced memory reactivation, cocaine-generated synapses are re-silenced, while cocaine seeking remains at high levels for a few hours. Bottom: when cocaine-generated synapses are re-silenced and weakened beforehand, cue re-exposure does not induce high-level cocaine seeking. Thus, cocaine-generated silent synapses are involved in the storage or reactivation of cocaine memories, while cocaine seeking expressed during the memory destabilization window is driven by an independent mechanism. See Supplementary Table 1 for exact P values for all comparisons made during post hoc tests. Data are presented as mean \pm s.e.m. Nontransduced.

The above results prompted us to test whether the decrease in active Rac1 destabilizes cocaine-generated synapses to allow their re-silencing after cue re-exposure (Fig. 4b). We thus used a herpes simplex virus (HSV) vector to express a dominant negative form

(dn) of Rac1, which interferes with the activity of endogenously active Rac1, in the NAcSh 45 d after cocaine self-administration. We then assessed silent synapses in HSV-infected MSNs ~12–16 h after viral injection (Fig. 4c,d). dnRac1 expression had no effect on



basal percentage of silent synapses in saline-trained rats (Fig. 4e,h and Supplementary Fig. 6a), indicating that dnRac1 expression alone does not generate silent synapses in the NAcSh of rats without cocaine experience. In contrast, silent synapses re-emerged in dnRac1-expressing NAcSh MSNs in cocaine-trained rats (Fig. 4f,h and Supplementary Fig. 6b,c), to levels similar to those restored in non-transduced MSNs by NASPM (Fig. 4h and Supplementary Fig. 6d). Additionally, application of NASPM did not further affect the percentage of silent synapses in dnRac1-expressing MSNs (Fig. 4g,h), suggesting that the silent synapses observed after dnRac1 were the same set of cocaine-generated silent synapses. These effects of dnRac1 are not likely due to nonspecific effects of HSV transduction or protein overexpression since a control HSV (HSV-C450M), which expresses a mutant, nonfunctional form of Rac1, exerted no effect on silent synapses (Supplementary Fig. 7).

While HSV expression of dnRac1 ensures sufficient Rac1 inhibition, it does not effectively capture the rapid temporal dynamics of synaptic re-silencing that naturally occur following cue re-exposure. To manipulate dnRac1 in a temporally controlled manner, we expressed a photoactivatable form of dnRac1 (pa-dnRac1), in which dnRac1 is fused with a photoreactive light oxygen voltage (LOV) domain, which prevents dnRac1 from interacting with its effectors^{32,33} (Fig. 4i–k). On exposure to 473-nm laser, the LOV domain dissociates from dnRac1, allowing dnRac1 to interfere

with the activity of endogenous Rac1 in a temporally controlled manner (Fig. 4k).

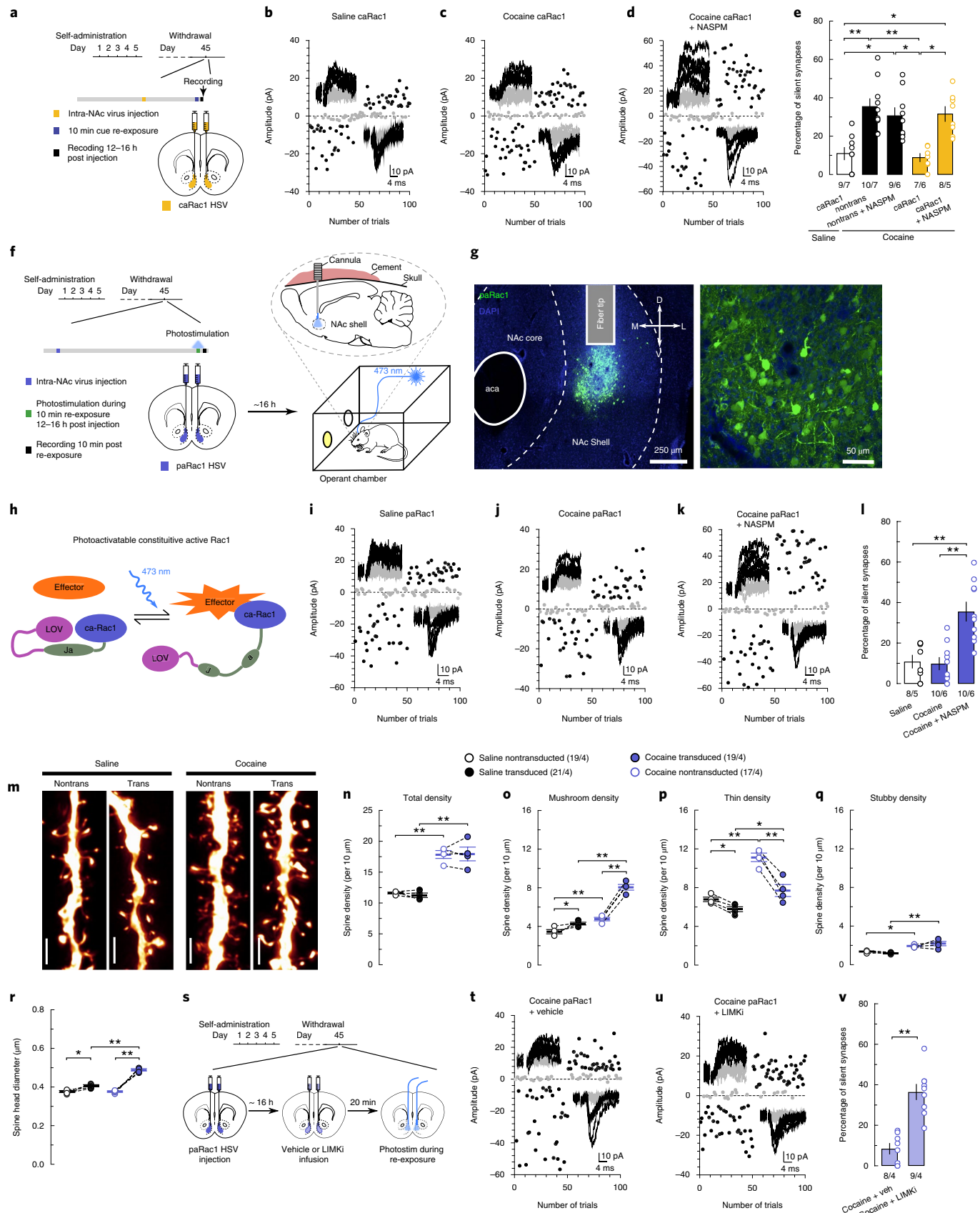
On withdrawal day 45, we injected HSV-pa-dnRac1 bilaterally into the rat NAcSh, and 12–16 h later, inserted optical fibers into NAcSh through preinstalled guide cannulae (Fig. 4i,j). We photo-stimulated NAcSh pa-dnRac1 for 10 min while rats were in their home cages, and assessed for silent synapses in transduced neurons immediately after. This manipulation did not affect the percentage of silent synapses in saline-trained rats (Fig. 4l,o and Supplementary Fig. 6e), but increased the percentage of silent synapses in cocaine-trained rats (Fig. 4m,o and Supplementary Fig. 6f). Furthermore, application of NASPM did not additionally change this percentage of silent synapses (Fig. 4n,o), again suggesting that silent synapses observed after dnRac1 stimulation were the same, cocaine-generated synapses. Taken together, a transient decrease in active Rac1 levels is sufficient to destabilize cocaine-generated synapses from the matured state for re-silencing.

We used cue-induced cocaine seeking as a final behavioral readout, which is presumably driven by several interwoven mechanisms and factors, including the memory intensity, memory reactivation efficacy and intermediate steps of memories that drive the ongoing behaviors. To gain insight into which mechanisms involve silent synapses, we measured cocaine seeking 2 h after cue re-exposure, when cocaine-generated synapses were in their re-silenced state.



Cocaine-trained rats exhibited high levels of cocaine seeking at this time point (Fig. 4p and Supplementary Fig. 6g). This result dissociates the dynamics of silent synapses from the ongoing expression

of cocaine seeking during the memory destabilization window. Indeed, similar dissociation is also observed in fear memories, in which the behavioral readout of fear memories remains at high



levels during the destabilization window after memory reactivation³⁴. Therefore, the state of NAcSh silent synapses does not determine the expression of cocaine seeking once the memories are reactivated. In contrast, when using pa-dnRac1 to manipulate the state of cocaine-generated synapses, we observed that re-silencing these synapses before, but not after, cue re-exposure-induced memory reactivation reduced cocaine seeking (Fig. 4q and Supplementary Fig. 6j–p). Thus, the state of cocaine-generated NAcSh synapses may preferentially control the intensity of stored memories or memory reactivation processes, while, once activated, the behavioral expression of these memories during the destabilization window is driven by other processes (Fig. 4r).

High levels of active Rac1 stabilize synaptic state. We next tested whether maintaining high levels of active Rac1 prevents the re-silencing of cocaine-generated synapses in response to cue re-exposure. We expressed a constitutively active mutant (ca) of Rac1, which is locked within its active conformation³¹. At 12–16 h after intra-NAcSh injection of HSV-caRac1, saline- or cocaine-trained rats received cue re-exposure (on withdrawal day 45) and were assessed for silent synapses 10 min later (Fig. 5a). Expression of

caRac1 did not affect the percentage of silent synapses in saline-trained rats with cue re-exposure (Fig. 5b,e and Supplementary Fig. 8a,c), but prevented cue re-exposure-induced re-emergence of silent synapses in cocaine-trained rats (Fig. 5c,e and Supplementary Fig. 8b–d). Application of NASPM restored the high percentage of silent synapses in caRac1-expressing MSNs (Fig. 5d,e and Supplementary Fig. 8e), indicating that cocaine-generated silent synapses were stabilized in their unsilenced, mature state. Thus, maintaining high levels of active Rac1 prevents the re-silencing of cocaine-generated synapses after memory retrieval.

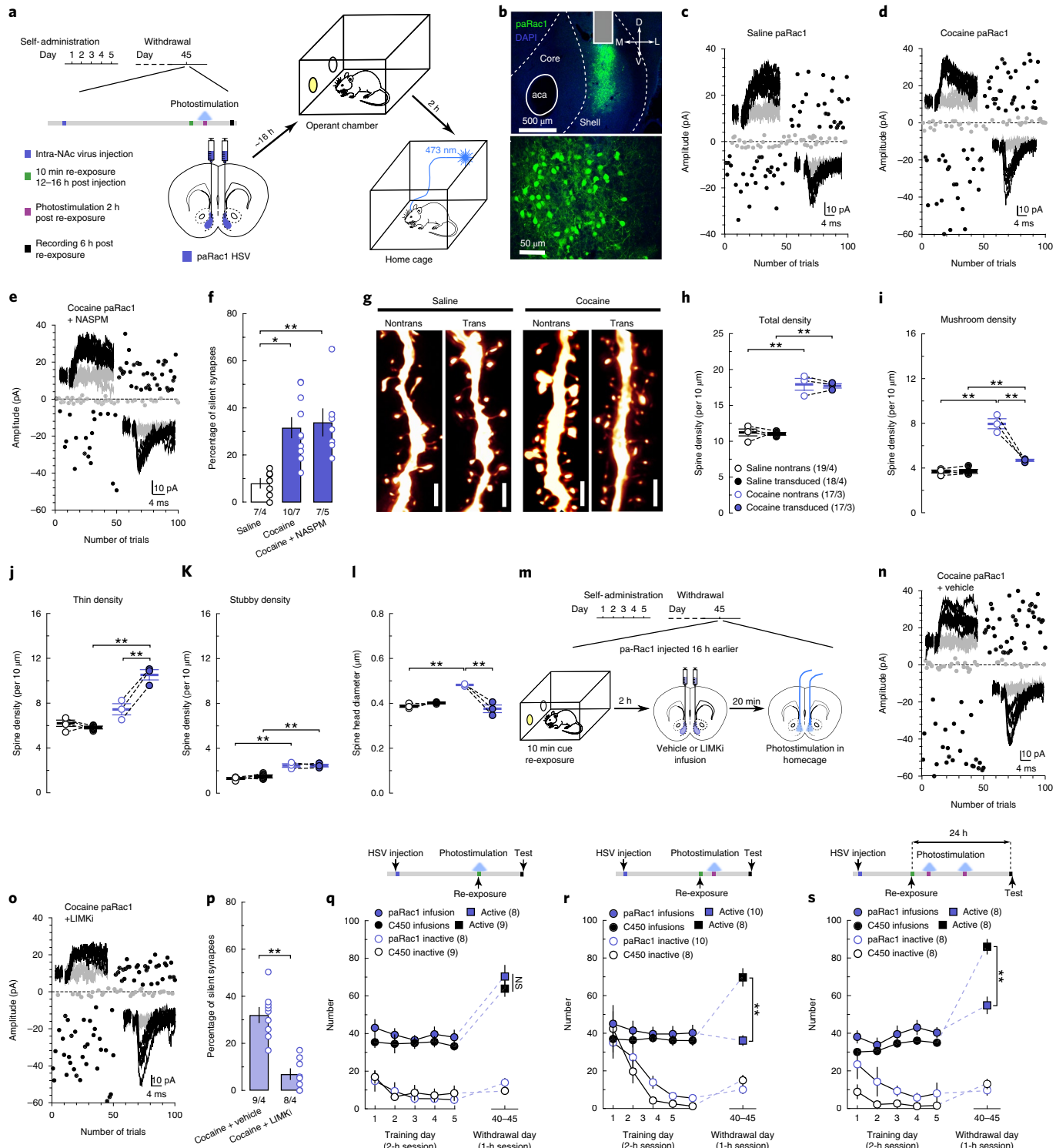
To characterize Rac1's temporally dynamic regulation, we employed a photoactivatable form of caRac1 (HSV-paRac1 (ref. ³¹)) (Fig. 5f–h). On withdrawal day 45, we injected HSV-paRac1 bilaterally in the NAcSh, and 12–16 h later, inserted optical fibers through preinstalled guide cannulae (Fig. 5f,g). Stimulation of NAcSh paRac1 during cue re-exposure did not affect the percentage of silent synapses in saline-trained rats (Fig. 5i,l and Supplementary Fig. 8f–h), but prevented the cue re-exposure-induced increase in the percentage of silent synapses in cocaine-trained rats (Fig. 5j,l and Supplementary Fig. 8f–h). The low percentage of silent synapses in these paRac1 MSNs was restored to high levels by



application of NASPM (Fig. 5k,l), indicating that the cocaine-generated synapses were not eliminated but stabilized in the unsilenced state with CP-AMPARs when high levels of active Rac1 were maintained.

Our subsequent spine morphology results mirror the electrophysiological findings. Specifically, stimulation of paRac1 did not change the density of total spines in either saline- or cocaine-trained rats compared with nontransduced MSNs within the same rats (Fig. 5m,n and Supplementary Fig. 8l–n). However, cue re-exposure-contingent paRac1 stimulation maintained the high

density of mushroom-like spines and low density of thin spines in cocaine-trained rats during the subsequent destabilization window (Fig. 5o,p), preventing the spine-weakening process induced by cue re-exposure (Fig. 2). Consistently, photostimulation also maintained the high mean spine head diameter of dendritic spines in paRac1-expressing MSNs, compared with nontransduced MSNs in the same cocaine-trained rats with cue re-exposure (Fig. 5r). Note that paRac1 stimulation also slightly affected the spine densities and spine head diameter in saline-trained rats (Fig. 5o–r), but these potentially nonspecific effects (~5%) are rather minimal and,



in our view, do not confound the interpretation of our results from cocaine-trained rats.

PAK-LIMK-cofilin signaling serves as a key mechanistic pathway through which active Rac1 suppresses actin depolymerization and stabilizes synapses³⁰. To test whether this pathway is utilized by paRac1 to prevent the re-silencing of cocaine-generated synapses following cue re-exposure, we infused a LIMK inhibitor (LIMKi) into the NAcSh ~20 min before photostimulation to disconnect the link between LIMK and Rac1 (Fig. 5s). In cocaine-trained rats with vehicle infusion, paRac1 stimulation prevented the re-emergence of silent synapses after cue re-exposure (Fig. 5t,v and Supplementary Fig. 8i-k). However, paRac1 stimulation could no longer prevent cue re-exposure-induced re-emergence of silent synapses in cocaine-trained rats given intra-NAcSh LIMKi infusion (Fig. 5u,v). These results suggest that active Rac1 stabilizes cocaine-generated synapses through the LIMK-cofilin pathway-mediated regulation of actin skeleton.

Stabilizing cocaine-generated synapses in the weakened state. The above results show that, while a decrease in active Rac1 triggers dynamic changes (silencing) in the synaptic state of cocaine-trained rats, maintaining high levels of active Rac1 locks synapses in their current mature state despite cue re-exposure. We thus asked whether active Rac1 can also lock cocaine-generated synapses within the weakened state once they are re-silenced after cue re-exposure. We again used HSV-paRac1 to stimulate Rac1 activity in cocaine-trained rats but 2 h after cue re-exposure, when cocaine-generated synapses are re-silenced (Fig. 6a,b), and assessed silent synapses 6 h later, when cocaine-generated synapses normally return to a mature state. We observed that the percentage of silent synapses was not affected in saline-trained rats (Fig. 6c,f and Supplementary Fig. 9a-c), but maintained at high levels in cocaine-trained rats (Fig. 6d,f). In addition, the percentage of silent synapses was not further increased on NASPM application (Fig. 6e,f). Thus, after cocaine-generated synapses are re-silenced by cue re-exposure, a high level of Rac1 is capable of maintaining them in the silent state.

Following the same paRac1-cue procedures, MSNs with paRac1 stimulation exhibited similar density of total spines (Fig. 6g,h and Supplementary Fig. 9g-i), but lower densities of mushroom-like spines (Fig. 6g,i) and higher densities of thin spines, compared with nontransduced MSNs from the same rats (Fig. 6g,j). The concurrent downshift of mushroom-like and upshift of thin spines suggest that cocaine-generated synapses weakened by cue re-exposure were stabilized in the weakened state. This conclusion is further supported by observations of decreased mean spine head diameter in MSNs with paRac1 stimulation (Fig. 6l). Meanwhile, paRac1 stimulation did not affect any dendritic spine subtypes in saline-trained rats (Fig. 6g-k).

As for locking mature synapses, the PAK-LIMK-cofilin pathway is also essential for active Rac1 to lock cocaine-generated synapses within a silent, weakened state (Fig. 6m). In cocaine-trained rats, intra-NAcSh infusion of LIMKi, but not vehicle, ~20 min before photostimulation prevented paRac1 from maintaining high levels of silent synapses beyond the 6 h destabilization window (Fig. 6n-p and Supplementary Fig. 9d-f). Thus, the same cytoskeleton-regulating pathway is employed by active Rac1 to lock cocaine-generated synapses in their current state, regardless of whether they are in a silent or unsilenced state. It is worth noting that the PAK-LIMK-cofilin pathway *in vivo* likely responds to the fluctuations of active Rac1 levels in a highly dynamic and complicated manner. As such, intervention of this pathway with different timing may result in different synaptic consequences.

If the functional state of cocaine-generated synapses in the NAcSh dictates the strength or reactivation of cocaine memories as hypothesized, locking synapses in their mature and silent states should preserve and compromise the behavioral outputs of cocaine

memories, respectively. To test this idea, we first stabilized cocaine-generated synapses in their mature state by stimulating paRac1 in cocaine-trained rats during cue re-exposure (Fig. 5f), and measured cue-induced cocaine seeking 6 h later (Fig. 6q). Cocaine-trained rats that received this paRac1 stimulation exhibited high cocaine seeking, comparable to control rats (with the same cocaine and photostimulation procedures, but expressing the control HSV-C450M) (Fig. 6q and Supplementary Figs. 10d and 11d-f,j-l). As an additional control, paRac1 stimulation also did not affect operant responding in saline-trained rats (Supplementary Figs. 10a-c and 11a-c,g-i). In contrast, when we stabilized cocaine-generated synapses in their silent state by stimulating paRac1 2 h after cue re-exposure (Fig. 6a), cue-induced cocaine seeking was decreased, compared with C450M control rats when measured 6 h after cue re-exposure (Fig. 6r and Supplementary Figs. 10h and 12d-f,j-l). This manipulation did not affect operant responding in saline-trained rats (Supplementary Figs. 10e-g and 12a-c,g-i).

To examine whether this potential anti-relapse effect of paRac1 was due to long-term memory alteration, we tested another set of cocaine-trained rats with two paRac1 stimulations within the destabilization window (2 and 5 h after cue re-exposure). These rats exhibited lower levels of cue-induced cocaine seeking compared with C450 control rats when measured >24 h after cue re-exposure (Fig. 6s and Supplementary Figs. 10i and 13). Thus, stabilizing cocaine-generated synapses in a silent state through paRac1 undermines the intensity or reactivation of cocaine memories, leading to decreased cocaine seeking.

Discussion

The synaptic mechanisms underlying destabilization and reconsolidation of drug-associated memories remain largely elusive. Our current findings provide such a mechanism, in which the dynamic state of a specific population of synapses, initially generated by cocaine experience, controls the destabilization and reconsolidation of cocaine memories. We propose that these cocaine-generated synapses represent a discrete synaptic ensemble through which key aspects of cocaine-associated memories can be manipulated for therapeutic benefit.

Silent synapses regulate cocaine memories. Memories are not static. After formation and consolidation, stabilized memories can be destabilized again on memory retrieval, followed by reconsolidation⁴. The destabilization not only allows for updating memories in response to changing outcomes, but also provides a therapeutic opportunity to weaken undesirable memories^{7,35}. Although synapses are important memory-encoding substrates, how synapses operate to mediate these memory dynamics remains elusive. AMPAR-silent excitatory synapses are generated in the NAcSh when rats acquire cue-conditioned cocaine self-administration, and then mature over prolonged withdrawal as cue-induced cocaine seeking strengthens^{16,18}. Here, we demonstrate that these synapses are re-silenced and weakened on memory destabilization following memory reactivation, and then re-mature when the memory reconsolidates (Fig. 1). When these synapses are held in the silent state after memory retrieval-induced re-silencing, reconsolidation is compromised, resulting in decreased cocaine seeking (Figs. 3 and 6). These findings depict cocaine-generated silent synapses as key cellular substrates underlying the dynamic process of memory destabilization and reconsolidation. As such, cocaine memories, and possibly other memories as well, can be mechanistically manipulated through specific underlying populations of synapses during the memory destabilization window, during which these synapses are naturally destabilized and primed for modification.

During the destabilization window, while cocaine-generated synapses are in a silent state, cue-induced cocaine seeking remains substantially elevated. However, when cocaine-generated synapses were

silenced before memory reactivation, cue-induced cocaine seeking was decreased^{16,18} (Figs. 3, 4 and 6). Thus, a dissociation between the functional state of cocaine-generated synapses and behavioral expression of cocaine memories emerges. We hypothesize that cocaine-generated synapses are key substrates for the storage or reactivation of cocaine memories; once the memories are reactivated, the behavioral expression is maintained by an independent set of mechanisms. This hypothesis explains high levels of cocaine seeking during the memory destabilization window in our current studies of cocaine memories, as well as in studies of fear memories³⁴. This mechanistic dissociation is physiologically beneficial, as it allows for the memory-encoding substrates to be destabilized for modification without sacrificing the ongoing behavioral output.

Projections from limbic and paralimbic regions form heterogeneous excitatory synapses onto NAc MSNs, regulating a wide range of emotional, motivational and cognitive responses³⁶. Drug addiction is expressed as alterations in selective, but not all, aspects of behavioral responses². It is thus expected that, while cocaine memories can be encoded in many of these afferents, within an individual projection, only a select population of synapses contributes to cocaine memories³⁷. Our present study randomly sampled silent synapses, presumably from all main NAc excitatory inputs that likely encompass many different aspects of cocaine memories. We have previously found that cocaine experience generates silent synapses in all NAc afferents examined^{16,17,38}, and silent synapses in these distinct projections have different behavioral influences¹⁷. Therefore, silent synapses within individual projections may encode specific aspects of cocaine memories, while collectively these synapses encode broader, multifaceted cocaine memories. Sharing similar biophysical and biochemical properties, cocaine-generated synapses across different NAc afferents as a whole can be collectively manipulated to maximize therapeutic benefit.

Signaling substrates governing synaptic state. Once formed, synapses can be held in a highly stable state for a lifetime, or destabilized and eliminated during memory retrieval and reconsolidation³⁹. The stability of synapses is finely controlled by signaling molecules, among which Rho family GTPases, particularly Rac1 (refs. 31,40,41), control focal changes in activated synapses⁴². Following cocaine memory retrieval, the level of active Rac1 transiently decreases, and mimicking this decrease destabilizes cocaine-generated synapses (Fig. 4). Conversely, increasing active Rac1 levels prevents the natural re-silencing of cocaine-generated synapses after memory retrieval (Fig. 5). These findings suggest that active Rac1 stabilizes synapses, while dynamic decreases in active Rac1 levels destabilize synapses for modification. Importantly, restoring high levels of active Rac1 during the destabilization window is also capable of stabilizing cocaine-generated synapses in their silent state (Fig. 6), indicating that active Rac1 stabilizes synapses in their current state, irrespective of whether they are in a weakened or strengthened state. In this case, Rac1-based manipulations might be developed to turn on and off the silent synapse-based memory destabilization window at intended time points beyond the classical 6-h window for therapeutic need.

Our findings that Rac1 stabilizes the synaptic state are consistent with the general role of Rac1 in regulating synaptic scaffolds. Specifically, Rac1 activates the PAK-LIMK signaling pathway (Figs. 5 and 6), which inhibits cofilin³⁰. Cofilin regulates the actin cytoskeleton by two main mechanisms: actin severing, and increasing the off-rate of actin monomers, both favoring actin depolymerization³⁰. However, actin severing also generates free barbed ends for elaboration and polymerization of actin, favoring actin polymerization⁴³. Thus, the dynamic balance between these two processes determines how a change in Rac1-cofilin signaling affects the current synaptic state. In mature and stably functioning synapses, the level of active Rac1 is often persistently high⁴⁴, resulting in

persistent inhibition of cofilin that prevents both actin depolymerization-mediated structural shrinkage and actin polymerization-mediated enlargement. Such a high stability of actin scaffolding and synaptic structure favors AMPARs to be maintained within the postsynaptic density³⁰ and molecular trafficking to be confined within the synapse⁴⁵, promoting the functional stability of synapses. In contrast, a decrease in active Rac1 levels is required for synaptic changes, such as generation and potentiation of new synapses after cocaine experience, but maintaining high levels of active Rac1 prevents this synaptic remodeling³¹. Based on these results and analyses, we interpret the role of Rac1 after cocaine withdrawal such that a decrease in active Rac1 levels is a permissive step for CP-AMPAR internalization, while the CP-AMPAR internalization is driven by Rac1-independent mechanisms.

Complexities of cocaine memories. Cocaine-associated memories are complex and contain information related to unconditioned responses, conditioned stimuli, motivational attributes and action, which involve diverse brain regions. These different memory components are not reactivated in isolation in our experimental set-ups as the rats are exposed to the cues and context, and allowed to respond operantly. Therefore, our results do not specify which specific components of cocaine memories are controlled by cocaine-generated synapses. However, significant clues exist. Specifically, previous results suggest that, rather than the conditioned stimulus (CS)–unconditioned stimulus (US) reconsolidation of cocaine memories^{46,47}, the NAc may preferentially encode the motivational attributes and CS–action association components of memories^{47,48}, leading to our speculation that NAc silent synapses are preferentially involved in the motivational and action-related aspects of cocaine memories.

When evaluating the translational potential of our current findings, boundary effects should be considered. While the training procedures used in the current study produce robust and persistent memories and ‘incubated’ drug seeking (Fig. 1)^{16–18} typically seen after extensive exposure to drugs^{19,23}, they do not adequately model the overtraining that occurs in human subjects with years of drug taking¹⁹. Overtraining can produce memories that are resistant to destabilization on traditional memory reactivation⁴⁹. Such boundary conditions may explain some discrepancies in the literature using different training procedures and test memory performance at different time points after acquisition^{46,47}, since boundary conditions can be transient⁵⁰. It is important for future studies to determine whether such boundary conditions result from impaired re-silencing of cocaine-generated synapses and, importantly, whether NAc silent synapses remain as effective anti-relapse targets after cocaine overtraining.

Concluding remarks. Cocaine-generated silent synapses are sparsely distributed across several NAc afferents, but collectively form a unique synaptic population, whose dynamic changes control the encoding, destabilization and reconsolidation of cocaine memories. These synapses may represent a discrete synaptic engram, with which cocaine memories are stored, retrieved and reconsolidated, and can be potentially targeted for clinical benefits.

Online content

Any methods, additional references, Nature Research reporting summaries, source data, extended data, supplementary information, acknowledgements, peer review information; details of author contributions and competing interests; and statements of data and code availability are available at <https://doi.org/10.1038/s41593-019-0537-6>.

Received: 25 November 2018; Accepted: 10 October 2019;
Published online: 2 December 2019

References

1. Hyman, S. E., Malenka, R. C. & Nestler, E. J. Neural mechanisms of addiction: the role of reward-related learning and memory. *Annu. Rev. Neurosci.* **29**, 565–598 (2006).
2. Wolf, M. E. Synaptic mechanisms underlying persistent cocaine craving. *Nat. Rev. Neurosci.* **17**, 351–365 (2016).
3. Nader, K. & Hardt, O. A single standard for memory: the case for reconsolidation. *Nat. Rev. Neurosci.* **10**, 224–234 (2009).
4. Tronson, N. C. & Taylor, J. R. Molecular mechanisms of memory reconsolidation. *Nat. Rev. Neurosci.* **8**, 262–275 (2007).
5. Lee, J. L. C., Di Ciano, P., Thomas, K. L. & Everitt, B. J. Disrupting reconsolidation of drug memories reduces cocaine-seeking behavior. *Neuron* **47**, 795–801 (2005).
6. Miller, C. A. & Marshall, J. F. Molecular substrates for retrieval and reconsolidation of cocaine-associated contextual memory. *Neuron* **47**, 873–884 (2005).
7. Torregrossa, M. M. & Taylor, J. R. Neuroscience of learning and memory for addiction medicine: from habit formation to memory reconsolidation. *Prog. Brain Res.* **223**, 91–113 (2016).
8. Jobes, M. L. et al. Effects of prereactivation propranolol on cocaine craving elicited by imagery Script/Cue sets in opioid-dependent polydrug users: a randomized study. *J. Addict. Med.* **9**, 491–498 (2015).
9. Lonergan, M. et al. Reactivating addiction-related memories under propranolol to reduce craving: a pilot randomized controlled trial. *J. Behav. Ther. Exp. Psychiatry* **50**, 245–249 (2016).
10. Dunbar, A. B. & Taylor, J. R. Reconsolidation and psychopathology: moving towards reconsolidation-based treatments. *Neurobiol. Learn. Mem.* **142**, 162–171 (2017).
11. Dong, Y. & Nestler, E. J. The neural rejuvenation hypothesis of cocaine addiction. *Trends Pharmacol. Sci.* **35**, 374–383 (2014).
12. Huang, Y. H. et al. In vivo cocaine experience generates silent synapses. *Neuron* **63**, 40–47 (2009).
13. Brown, T. E. et al. A silent synapse-based mechanism for cocaine-induced locomotor sensitization. *J. Neurosci.* **31**, 8163–8174 (2011).
14. Isaac, J. T., Nicoll, R. A. & Malenka, R. C. Evidence for silent synapses: implications for the expression of LTP. *Neuron* **15**, 427–434 (1995).
15. Liao, D., Hessler, N. A. & Malinow, R. Activation of postsynaptically silent synapses during pairing-induced LTP in CA1 region of hippocampal slice. *Nature* **375**, 400–404 (1995).
16. Lee, B. R. et al. Maturation of silent synapses in amygdala-accumbens projection contributes to incubation of cocaine craving. *Nat. Neurosci.* **16**, 1644–1651 (2013).
17. Ma, Y.-Y. et al. Bidirectional modulation of incubation of cocaine craving by silent synapse-based remodeling of prefrontal cortex to accumbens projections. *Neuron* **83**, 1453–1467 (2014).
18. Ma, Y.-Y. et al. Re-silencing of silent synapses unmasks anti-relapse effects of environmental enrichment. *Proc. Natl Acad. Sci. USA* **113**, 5089–5094 (2016).
19. Grimm, J. W., Hope, B. T., Wise, R. A. & Shaham, Y. Neuroadaptation. Incubation of cocaine craving after withdrawal. *Nature* **412**, 141–142 (2001).
20. Graziane, N. M. et al. Opposing mechanisms mediate morphine- and cocaine-induced generation of silent synapses. *Nat. Neurosci.* **19**, 915–925 (2016).
21. Hanse, E., Seth, H. & Riebe, I. AMPA-silent synapses in brain development and pathology. *Nat. Rev. Neurosci.* **14**, 839–850 (2013).
22. Cull-Candy, S., Kelly, L. & Farrant, M. Regulation of Ca^{2+} -permeable AMPA receptors: synaptic plasticity and beyond. *Curr. Opin. Neurobiol.* **16**, 288–297 (2006).
23. Conrad, K. L. et al. Formation of accumbens GluR2-lacking AMPA receptors mediates incubation of cocaine craving. *Nature* **454**, 118–121 (2008).
24. Nader, K., Schafe, G. E. & LeDoux, J. E. Fear memories require protein synthesis in the amygdala for reconsolidation after retrieval. *Nature* **406**, 722–726 (2000).
25. Holtmaat, A. & Svoboda, K. Experience-dependent structural synaptic plasticity in the mammalian brain. *Nat. Rev. Neurosci.* **10**, 647–658 (2009).
26. Matsuzaki, M. et al. Dendritic spine geometry is critical for AMPA receptor expression in hippocampal CA1 pyramidal neurons. *Nat. Neurosci.* **4**, 1086–1092 (2001).
27. Lin, M. T. et al. Coupled activity-dependent trafficking of synaptic SK2 channels and AMPA receptors. *J. Neurosci.* **30**, 11726–11734 (2010).
28. Hayashi, Y. et al. Driving AMPA receptors into synapses by LTP and CaMKII: requirement for GluR1 and PDZ domain interaction. *Science* **287**, 2262–2267 (2000).
29. Zhou, Z. et al. The C-terminal tails of endogenous GluA1 and GluA2 differentially contribute to hippocampal synaptic plasticity and learning. *Nat. Neurosci.* **21**, 50–62 (2018).
30. Cingolani, L. A. & Goda, Y. Actin in action: the interplay between the actin cytoskeleton and synaptic efficacy. *Nat. Rev. Neurosci.* **9**, 344–356 (2008).
31. Dietz, D. M. et al. Rac1 is essential in cocaine-induced structural plasticity of nucleus accumbens neurons. *Nat. Neurosci.* **15**, 891–896 (2012).
32. Wu, Y. I. et al. A genetically encoded photoactivatable Rac controls the motility of living cells. *Nature* **461**, 104–108 (2009).
33. Wang, X., He, L., Wu, Y. I., Hahn, K. M. & Montell, D. J. Light-mediated activation reveals a key role for Rac in collective guidance of cell movement in vivo. *Nat. Neurosci.* **12**, 591–597 (2010).
34. Monfils, M.-H., Cowansage, K. K., Klann, E. & LeDoux, J. E. Extinction-reconsolidation boundaries: key to persistent attenuation of fear memories. *Science* **324**, 951–955 (2009).
35. Lee, J. L. C. Memory reconsolidation mediates the strengthening of memories by additional learning. *Nat. Neurosci.* **11**, 1264–1266 (2008).
36. Sesack, S. R. & Grace, A. A. Cortico-basal ganglia reward network: microcircuitry. *Neuropsychopharmacology* **35**, 27–47 (2010).
37. Cruz, F. C. et al. New technologies for examining the role of neuronal ensembles in drug addiction and fear. *Nat. Rev. Neurosci.* **14**, 743–754 (2013).
38. Neumann, P. A. et al. Cocaine-induced synaptic alterations in thalamus to nucleus accumbens projection. *Neuropsychopharmacology* **41**, 2399–2410 (2016).
39. Yang, G., Pan, F. & Gan, W.-B. Stably maintained dendritic spines are associated with lifelong memories. *Nature* **462**, 920–924 (2009).
40. Liao, Z. et al. Fear conditioning downregulates Rac1 activity in the basolateral amygdala astrocytes to facilitate the formation of fear memory. *Front. Mol. Neurosci.* **10**, 396 (2017).
41. Das, A., Dines, M., Alapin, J. M. & Lamprecht, R. Affecting long-term fear memory formation through optical control of Rac1 GTPase and PAK activity in lateral amygdala. *Sci. Rep.* **7**, 13930 (2017).
42. Nishiyama, J. & Yasuda, R. Biochemical computation for spine structural plasticity. *Neuron* **87**, 63–75 (2015).
43. Ghosh, M. et al. Cofilin promotes actin polymerization and defines the direction of cell motility. *Science* **304**, 743–746 (2004).
44. Yasuda, R. Biophysics of biochemical signaling in dendritic spines: implications in synaptic plasticity. *Biophys. J.* **113**, 2152–2159 (2017).
45. Obashi, K., Matsuda, A., Inoue, Y. & Okabe, S. Precise temporal regulation of molecular diffusion within dendritic spines by actin polymers during structural plasticity. *Cell Rep.* **27**, 1503–1515.e1508 (2019).
46. Wells, A. M. et al. Extracellular signal-regulated kinase in the basolateral amygdala, but not the nucleus accumbens core, is critical for context-response-cocaine memory reconsolidation in rats. *Neuropsychopharmacology* **38**, 753–762 (2013).
47. Theberge, F. R. M., Milton, A. L., Belin, D., Lee, J. L. C. & Everitt, B. J. The basolateral amygdala and nucleus accumbens core mediate dissociable aspects of drug memory reconsolidation. *Learn. Mem.* **17**, 444–453 (2010).
48. Everitt, B. J. & Robbins, T. W. Neural systems of reinforcement for drug addiction: from actions to habits to compulsion. *Nat. Neurosci.* **8**, 1481–1489 (2005).
49. Taylor, J. R., Olaussen, P., Quinn, J. J. & Torregrossa, M. M. Targeting extinction and reconsolidation mechanisms to combat the impact of drug cues on addiction. *Neuropharmacology* **56**, 186–195 (2009).
50. Wang, S.-H., de Oliveira Alvares, L. & Nader, K. Cellular and systems mechanisms of memory strength as a constraint on auditory fear reconsolidation. *Nat. Neurosci.* **12**, 905–912 (2009).

Publisher's note Springer Nature remains neutral with regard to jurisdictional claims in published maps and institutional affiliations.

© The Author(s), under exclusive licence to Springer Nature America, Inc. 2019

Methods

Subjects. Male Sprague-Dawley rats (postnatal day 35–40 with 130–150 g body weight on arrival) (Charles River) were used in all experiments. Rats were singly housed on a 12-h light/dark cycle (light on/off at 7:00/19:00) with food and water available ad libitum. Rats were allowed to habituate to their housing cages for ~1 week before the catheter surgery. All rats were used in accordance with protocols approved by the Institutional Care and Use Committees at the University of Pittsburgh and Icahn School of Medicine at Mount Sinai.

Catheter implantation. Self-administration surgery was performed as described previously^{16,51}. Briefly, a silastic catheter was inserted into the right jugular vein by 2.5 cm, and the distal end was led subcutaneously to the back between the scapulae. Catheters were constructed of silastic tubing (length, 10 cm; inner diameter, 0.0508 cm; outer diameter, 0.09398 cm) and connected to a commercially available Vascular Access Button (Instech). Rats were allowed to recover for 3–5 d after surgery. During the recovery period, the catheter was flushed daily with 1 ml kg⁻¹ heparin (10 U ml⁻¹) and gentamicin antibiotics (5 mg ml⁻¹) in sterile saline to minimize potential infection and catheter occlusion.

Self-administration apparatus. Behavioral experiments were conducted in operant-conditioning chambers enclosed within sound-attenuating cabinets (Med Associates). Each chamber (29.53 × 24.84 × 18.67 cm³) contains an active and an inactive nose poke hole, a food dispenser, a conditioned stimulus light in each nose poke hole and a house light. No food or water was provided in the chamber during the training or testing sessions.

Intravenous cocaine self-administration training. Cocaine self-administration training began ~5 d after surgery. On day 1, rats were placed in self-administration chambers for an overnight training session on a fixed ratio 1 reinforcement schedule. Nose poking in the active hole resulted in a cocaine infusion (0.75 mg kg⁻¹ over 3–6 s) and illumination of the conditioned stimulus light inside the nose poke hole as well as the house light. The conditioned stimulus light remained on for 6 s, whereas the house light was illuminated for 20 s, during which active nose pokes were counted but resulted in no cocaine infusions. After the 20-s timeout period, the house light was turned off, and the next nose poke in the active hole resulted in a cocaine infusion. Nose pokes in the inactive hole had no reinforced consequences but were recorded. Rats first underwent one overnight training session (~12 h) to facilitate acquisition. Only rats that received at least 80 cocaine infusions during the overnight session were allowed to receive the 5-d cocaine self-administration regimen (<2% of rats failed to meet this criteria). The same or similar self-administration procedures/standards were used in our previous studies^{16,18,51}. On the fifth day of training, rats were placed back into their home cages and remained there during subsequent withdrawal days. Cocaine-trained rats that failed to meet self-administration criteria (≥ 15 infusions per session, 70% active-to-inactive nose poke response ratio) were excluded from further experimentation and analysis. Note that rats with high inactive nose pokes relative to active were excluded as the inactive nose poke responding likely reflected unconditioned motor-stimulating effects (for example, stereotypic biting of nose poke hole) rather than learned operant responses.

Withdrawal phase. Rats were returned to their home cages after each cocaine self-administration session. After the 5-d procedure, the rats were singly housed in their home cages for drug withdrawal, with food and water available ad libitum. Withdrawal day 1 was operationally defined as 20–26 h after the last session of cocaine self-administration. Withdrawal day 45 was operationally defined as 40–48 d after the last session of cocaine self-administration.

Memory retrieval. Cue-induced memory retrieval sessions were performed in the same manner as the cue-induced cocaine-seeking procedure as detailed below, except that the sessions lasted for 10–15 min.

Cue-induced cocaine seeking. Cue-induced cocaine seeking was assessed in an extinction test (1 h) conducted after 1-d or 45-d withdrawal from cocaine self-administration. During the extinction test session, active nose pokes resulted in contingent deliveries of the conditioned stimulus light cues but not cocaine. The number of nose pokes to the active holes was used to quantify cue-induced cocaine seeking, and the number of nose pokes to the inactive holes was used as control.

GluA1 peptide. The peptide TGL (SSGMPLGATGL) was used to interfere with GluA1 subunit-containing AMPAR trafficking. A similar peptide AGL (SSGMPLGAAGL) was used as the control for TGL. AGL has a single different amino acid that prevents the peptide from interfering with GluA1 (ref. ²⁷). These two peptides were conjugated with a trans-activating transcriptional activator (TAT) sequence (GRKKRRQRRRPQ) to facilitate intracellular delivery, resulting in TAT-pep1-TGL (GRKKRRQRRRPQSSGMLGATGL) and TAT-pep1-AGL (GRKKRRQRRRPQSSGMLGAAGL). TAT-TGL and TAT-AGL were custom-made from GenScript.

Peptide and LIMKi injections. For peptide injections, on withdrawal day 35, rats (350–400 g) were bilaterally implanted with guide cannulae (Plastics One) targeting the NAcSh (in mm: anterior-posterior (AP), +1.60; medial-lateral (ML), ±1.00; dorsal-ventral (DV), -6.80). On withdrawal day 45, at the specified time point (for example, 2 or 6 h) after cue re-exposure, rats were lightly anesthetized and peptide (30 µM) was infused through 32-gauge needles extending 1 mm below the cannula into the NAcSh (in mm: AP, +1.60; ML, ±1.00; DV, -7.80). For electrophysiological experiments, 1 µl per side (30 pmol per side) was injected to maximize peptide spread throughout the recording area. For behavioral experiments, 0.5 µl per side (15 pmol per side) was injected to ensure the NAcSh-confined effects. Peptide was infused at a rate of 200 nl min⁻¹, and the infusing needle was left in place for 5 min to minimize backflow. Based on injections of EvansBlue dye, 1-µl infusions diffused throughout the NAcSh and into the NAc core, and 0.5-µl infusions were confined within the NAcSh. In addition, previous studies using similar peptides and TAT sequences confirm that the vast majority of neurons within the infusion area take up the peptide³². For electrophysiology experiments, to ensure that recordings were made from MSNs within the infusion area, all recordings were made within the ~200-µm radius from the center of the injection site, an area well within the boundaries covered by the infusion. The injection sites of each rat for behavioral tests were assessed by injecting 0.5-µl EvansBlue dye using the same approach as for peptide injections. Rats were subsequently decapitated under deep isoflurane anesthesia and coronal slices (300 µm thick) containing NAc were prepared on a VT1200S vibratome (Leica) in PBS. Localizations of EvansBlue dye were determined visually and recorded. Rats with inaccurate injections were excluded from data analysis.

To manipulate the PAK-LIMK-cofilin pathway in vivo, we infused CRT0105950 (Tocris), a highly selective LIMK1/2 inhibitor (LIMKi)⁵³. LIMKi was dissolved in 1% dimethylsulfoxide and 0.1 M Dulbecco's sterile PBS. We used 1% dimethylsulfoxide and 0.1 M Dulbecco's sterile PBS as the vehicle control. Infusion of the LIMKi to the NAcSh was performed as described for the peptide infusions. Briefly, LIMKi at 10 µM (1 µl per side), a dose shown to sufficiently inhibit LIMK with minimal negative effects on cell viability⁵³, was infused into the NAcSh through a preinstalled cannula at a rate of 200 nl min⁻¹. Similar to peptide experiments, all electrophysiology recordings were performed within the 200-mm radius of the injection center.

Viral vectors and delivery. We used the bicistronic p1005 HSV vector to express dnRac1, caRac1, Rac1-C450M (control), pa-dnRac1 and paRac1 combined with green fluorescent protein (GFP) or mCherry, as described previously^{31,32}. These HSVs were prepared using the same methods described previously^{31,54,55}. Earlier work shows that HSVs infect neurons only, and in the NAc, the vast majority of HSV-infected neurons are MSNs⁵⁶. In our recordings, we came across very few transduced inhibitory interneurons (~10 throughout the entire study) and no transduced cholinergic interneurons. Thus, effects mediated by HSV-mediated transduction are most attributable to MSNs.

Due to the rapid and transient HSV-mediated expression, rats were bilaterally implanted with guide cannulae (Plastics One) targeting the NAcSh on withdrawal day 35, as described above. Rats were injected with HSVs 12–16 h before electrophysiological or behavioral experiments on withdrawal day 45. During injection, rats were lightly anesthetized and HSV (1 µl per side) was bilaterally infused (100 nl min⁻¹) through 32-gauge needles extending 1 mm below the cannulae into the NAcSh (in mm: AP, +1.60; ML, ±1.00; DV, -7.80). Infusing needles were left in place for 10 min following injection to prevent backflow and allow for sufficient diffusion of HSV vectors away from the injection site. This approach minimized potential behavioral disturbance following acute intracranial surgeries and allowed for the insertion of optic fibers for the photoactivation experiments (see section “Photostimulation of paRac1”).

For electrophysiology experiments, viral injections and expression were visually verified in brain slices prepared for recording, while for behavioral experiments, immunohistochemistry and confocal microscopy (see section “Immunohistochemistry and confocal microscopy”) were used for verification. Rats with inaccurate injections or weak viral expression were excluded from data analysis.

Photoactivation of paRac1. The activity of paRac1 is sharply increased following photostimulation, and then decays exponentially with a half-life ($T_{1/2}$) ≈ 10 s at room temperature³². The decay kinetics are likely faster in vivo. We used a stimulation protocol composed of 473-nm laser pulses at frequency of 10 Hz, pulse duration of 0.5 ms and laser intensity of 10 mW mm⁻². Laser was generated and controlled by a 473-nm blue laser diode (IkeCool), and the pulse patterns were generated through a waveform isolator (A.M.P.I.). The photostimulation protocol was delivered for 10 min to match the duration of cue re-exposure. Stimulation parameters in this protocol have been verified to introduce minimal tissue damage in behaving rats in our previous studies⁵⁷, and were used in all photoactivation experiments presented in this manuscript.

For in vivo photostimulation experiments, rats were bilaterally implanted with guide cannulae (Plastics One) targeting the NAcSh (in mm: AP, +1.60; ML, ±1.00; DV, -6.00) on withdrawal day 35. For rats receiving photostimulation on withdrawal day 45, the rats were slightly restrained and two 200-µm-core optical fibers were bilaterally inserted through the cannulae. The length of the

optical fiber was adjusted such that the tip would rest ~300 μm dorsal to the viral injection site (in mm: AP, +1.60; ML, ±1.00; DV, −7.50). Immediately after the optical fiber was secured, the rat was placed back into its home cage (pa-dnRac1 in Fig. 4 and 2 h post paRac1 in Fig. 6) or in the operant chamber (paRac1 during re-exposure in Fig. 5), with the fiber attached to a tether system to allow rats free movement during photostimulation. After the stimulation session, the optical fibers were removed and the rat was placed back into its home cage. For behavioral experiments testing the effects of paRac1 activation 24 h after cue re-exposure, a second photostimulation session 5 h after cue re-exposure was performed to extend the duration of Rac1 activation within the destabilization window.

Rac1 assay. At specified time points, the rats were killed by decapitation, and the brain was quickly removed and snap-frozen in 2-methylbutane (Sigma Aldrich) for 1 min. Using a brain matrix, 2-mm-thick brain slices were prepared and tissue punches containing the NAc were extracted. The punched tissue was homogenized in lysis buffer (4°C) and then centrifuged at 14,000g for 2 min at 4°C. The supernatant was collected and snap-frozen. Lysate was stored at −80°C. Rac1-GTP was quantified with the Rac1 G-LISA Activation Assay (Absorbance Based; Cytoskeleton) according to the manufacturer instructions. Rac1-GTP levels were then assessed by the absorbance of each sample at 490 nm.

Preparation of acute brain slices. Rats were decapitated following isoflurane anesthesia. For NAc-containing slices, coronal slices (250 μm thick) containing the NAc were prepared on a VT1200S vibratome (Leica) in 4°C cutting solution containing (in mM): 135 N-methyl-d-glutamine, 1 KCl, 1.2 KH₂PO₄, 0.5 CaCl₂, 1.5 MgCl₂, 20 choline-HCO₃, and 11 glucose, saturated with 95% O₂/5% CO₂ and pH adjusted to 7.4 with HCl. Osmolality was adjusted to 305 mmol kg⁻¹. For hippocampal recordings, transverse slices (400 μm thick) containing the ventral hippocampus were prepared on a VT1200S vibratome (Leica) in 4°C cutting solution. A small cut was made in the CA3 region to prevent epileptic activities in the CA1 region. Slices were incubated in the artificial cerebrospinal fluid (aCSF) containing (in mM): 119 NaCl, 2.5 KCl, 2.5 CaCl₂, 1.3 MgCl₂, 1 NaH₂PO₄, 26.2 NaHCO₃ and 11 glucose, with the osmolality adjusted to 280–290 mmol kg⁻¹. Slices were placed in the aCSF saturated with 95% O₂/5% CO₂ at 37°C for 30 min and then held at 20–22°C for at least 30 min before experimentation.

Electrophysiological recordings. Extracellular field recordings. All field recordings were made within the CA1 region of the hippocampus. Before recordings, hippocampal slices were incubated with 200 μM TGL or 200 μM AGL for >1 h. During recordings, slices were superfused with high-divalent aCSF, containing the same ingredients as the holding aCSF except that 4 mM CaCl₂ and MgCl₂ were used to replace 2.5 mM CaCl₂ and 1.3 mM MgCl₂. Recordings were made by placing a recording electrode filled with 2 M NaCl in the stratum radiatum of the CA1. Schaffer collaterals originating from the CA3 were stimulated with a constant-current isolated stimulator (Digitimer), using a monopolar electrode (glass pipette filled with aCSF). Synaptic currents were recorded with a MultiClamp 700B amplifier, filtered at 2.6–3 kHz, amplified five times and then digitized at 20 kHz. A high-frequency stimulation (two 1-s trains at 100 Hz with a 20-s interval, 1.5 times the test current intensity) was used to induce LTP. In experiments involving inhibition of NMDARs, 50 μM (2R)-amino-5-phosphonovaleric acid (APV) was included in the bath.

Whole-cell recordings. All recordings were made from MSNs located in the medial NAcSh. During recordings, slices were superfused with aCSF, heated to 30–32°C by passing the solution through a feedback-controlled in-line heater (Warner) before entering the recording chamber. To measure minimal stimulation-evoked responses, electrodes (2–5 MΩ) were filled with a cesium-based internal solution (in mM: 135 CsMeSO₃, 5 CsCl, 5 TEA-Cl, 0.4 EGTA (Cs), 20 HEPES, 2.5 Mg-ATP, 0.25 Na-GTP, 1 QX-314 (Br), pH 7.3). Picrotoxin (0.1 mM) was included in the aCSF during all recordings to inhibit GABA_A receptor-mediated currents. Presynaptic afferents were stimulated by a constant-current isolated stimulator (Digitimer), using a monopolar electrode (glass pipette filled with aCSF). Series resistance was typically 7–20 MΩ, uncompensated and monitored continuously during recording. Cells with a change in series resistance >20% were excluded from data analysis. Synaptic currents were recorded with a MultiClamp 700B amplifier, filtered at 2.6–3 kHz, amplified five times and digitized at 20 kHz.

Detection of GluN2B-NMDAR currents. To measure NMDAR-mediated EPSCs, 2,3-dihydroxy-6-nitro-7-sulfamoyl-benzof[fl]quinoxaline (NBQX) (5 μM) and picrotoxin (0.1 mM) were included in the bath. Recorded neurons were held at −40 mV to partially relieve Mg²⁺-mediated blockage of NMDARs. Following a 7-min baseline recording, the bath that additionally contained the GluN2B-selective antagonist Ro256981 (200 nM) was switched in. NMDAR EPSCs were continuously recorded as the new bath perfused the slice, but only EPSCs after 8 min were included for data analysis to allow diffusion of Ro256981 into the slice and this use-dependent antagonist to operate. After 10 min of recording, a bath containing APV (50 μM) instead of Ro256981 was switched in to inhibit all NMDARs, which verified that recorded EPSCs were mediated by NMDARs.

Detection of CP-AMPARs. To isolate AMPAR-mediated EPSCs, picrotoxin (0.1 mM) and APV (50 μM) were included in the bath. To properly assess the

rectification of AMPAR EPSCs, spermine (0.1 mM) was freshly added to the internal solution. AMPAR EPSCs were evoked at progressively depolarized holding potentials (−70 mV to +50 mV with a 10-mV increment) to generate an *I*-*V* curve. Twelve responses were recorded at each holding potential and averaged. The rectification index was calculated by comparing the peak amplitude at +50 mV to −70 mV after correction for the reversal potential with the following equation:

$$\text{Rectification index} = (I_{+50}/(50 - E_R))/(I_{-70}/(-70 - E_R))$$

where *I* is the peak amplitude at either +50 mV or −70 mV, and *E_R* is the reversal potential of AMPAR EPSCs, which was measured manually for each recorded neuron.

Silent synapse recordings and analysis. NAcSh MSNs were randomly selected for recording. The minimal stimulation assay was performed as previously described^{12,14–16,18}. After obtaining small (~50 pA) EPSCs at −70 mV, the stimulation intensity was reduced in small increments to the point that failures versus successes of synaptically evoked events (EPSCs) could be clearly distinguished. The stimulation intensity and frequency were then kept constant for the rest of the experiment. The amplitudes of both AMPAR and NMDAR EPSCs resulting from single vesicular release are relatively large in NAcSh MSNs (for example, ~15 pA for AMPAR mEPSCs at −70 mV), which facilitates the judgment of successes versus failures. For each cell, 50–100 traces were recorded at −70 mV, and 50–100 traces were recorded at +50 mV. Recordings were then repeated at −70 mV and +50 mV for another round or two. Only cells with relatively constant failure rates (changes <15%) between rounds were used to assess percentage of silent synapses. We visually detected failures versus successes at each holding potential over 50–100 trials to calculate the failure rate, as described previously^{12,16,17}. We performed this analysis in a blind manner such that a small number of ambiguous responses were categorized in a fully unbiased way.

To quantify percentage of silent synapses, we made two theoretical assumptions: (1) the presynaptic release sites are independent, and (2) release probability across all synapses, including silent synapses, is identical. Thus, the percentage of silent synapses was calculated using the equation: $1 - \ln(F_{-70})/\ln(F_{+50})$, in which *F₋₇₀* was the failure rate at −70 mV and *F₊₅₀* was the failure rate at +50 mV, as rationalized previously¹⁵. Note that in this equation, the failure rate is the only variable that determines the percentage of silent synapses. The amplitudes of EPSCs are used to present failures or successes, but do not have analytical value. In the cases in which these two theoretical assumptions are not true, the above equation was still used, as the results were still valid in predicting the changes of silent synapses qualitatively as previously rationalized^{17,58}. The amplitude of an EPSC was determined as the mean value of the EPSC over a 1-ms time window around the peak, which was typically 3–4 ms after the stimulation artifact. To assess the percentage of silent synapses, only the rates of failures versus successes, not the absolute values of the amplitudes, were used. At +50 mV, successful synaptic responses were conceivably mediated by both AMPARs and NMDARs, and inhibiting AMPARs by NBQX (5 μM) modestly reduces the amplitudes of EPSCs²⁰. Despite the effects of NBQX on the amplitudes, the failure rate of synaptic responses at +50 mV was not altered during AMPAR inhibition²⁰. Thus, in the minimal stimulation assay assessing the percentage of silent synapses, the results will not be affected, whether the synaptic responses at +50 mV are mediated by NMDARs alone or by both AMPARs and NMDARs.

Immunohistochemistry and confocal microscopy. At 1–4 d after behavioral testing, when HSV expression remained readily detectable, rats were transcardially perfused with 0.1 M sodium phosphate buffer, followed by 4% paraformaldehyde (PFA, wt/wt) in 0.1 M phosphate buffer. Brains were removed and postfixed in 4% PFA overnight at 4°C. Following postfix, whole brains were stored in 30% sucrose in phosphate buffer with 0.1% sodium azide at 4°C until sectioning. Coronal sections (100 μm thick) containing the NAc were then prepared on a VT1200S vibratome (Leica) in 0.1 M PBS and then stored in cryoprotectant (30% sucrose, 30% ethylene glycol, in phosphate buffer) at −20°C until staining.

Immunohistochemistry was performed as previously described³⁹. Briefly, floating sections were washed in PBS 3 × 5 min and then permeabilized with 0.1% Triton X-100 in PBS for 15 min. Sections were then washed 3 × 5 min in PBS and blocked with 5% normal donkey serum in PBS for 2 h. Sections were next incubated overnight at 4°C with a primary antibody against GFP (1:1,000, monoclonal mouse anti-GFP; Abcam). Sections were subsequently washed 3 × 5 min in PBS and incubated for 2 h at room temperature with a secondary antibody (1:500, ALEXA 488 donkey anti-mouse; Abcam). Sections were washed again 3 × 5 min in PBS before they were mounted in ProLong Gold Antifade with DAPI (Molecular Probes).

Sections were imaged and captured with Leica TCS SP5 confocal microscope equipped with Leica Application Suite software (Leica). Slices were imaged with a 5x or 10x air objective and the entire slice was captured using automated tile scanning and image stitching functions. From these images, viral expression and localization could be determined. All representative images were captured with a 10x air objective. In addition, high-magnification images of transduced neurons were captured using a 40x oil immersion objective to verify viral expression in intact neurons.

Dendritic spine labeling and imaging. To visualize dendritic spines, MSNs were filled with Alexa 594 dye using single-cell microinjections, and the labeled dendritic spines were quantified as described previously^{60,61}. Briefly, the rats were transcardially perfused with ice-cold 1% PFA in 0.1 M phosphate buffer, followed by 4% PFA and 0.125% glutaraldehyde in 0.1 M phosphate buffer. Brains were removed and postfixed in 4% PFA and 0.125% glutaraldehyde in 0.1 M phosphate buffer for 12–14 h at 4°C. Following postfix, the brains were transferred into 0.1 M PBS and sectioned into 250-μm-thick slices using a VT1200S vibratome (Leica). Cells were filled shortly after slicing (within 4 h). Cells within the NAcSh were impaled with a fine micropipette containing 5 mM Alexa 594 hydrazide (Invitrogen) and injected with 1–10 nA of negative current until dendrites and spines were filled. Based on the presence of GFP signals, transduced and nontransduced cells were visually targeted and filled in the same rat. After filling, the slices were mounted in ProLong Gold Antifade (Molecular Probes) on slides for imaging. Spacers (240 μm thick) were placed along the edge of the slide before mounting to avoid compression of the slices by the overlying coverslip and to prevent deformation of spine morphologies.

Images were captured with a Leica TCS SP5 confocal microscope equipped with Leica Application Suite software (Leica). Individually filled neurons were visualized with a $\times 63$ oil immersion objective for final verification of their neuronal types (for example, MSNs versus interneurons). Individual dendritic segments were focused on and scanned at 0.69-μm intervals along the z axis to obtain a z-stack. After capture, all images were deconvolved within the Leica Application Suite software. Analyses were performed on two-dimensional projection images using ImageJ (NIH). Secondary dendrites were sampled and analyzed due to their significant cellular and behavioral correlates^{20,62}. For each neuron, 1–4 (2.1 average) dendritic segments of ~20 μm in length were analyzed. For each group, 4–8 cells per rat were analyzed. For experiments examining the effects of paRac1 stimulation, 4–8 nontransduced and 4–8 transduced cells were analyzed and compared from the same rat. Similar to our previous studies, we operationally divided spines into three categories^{15,20}: (1) mushroom-like spines were dendritic protrusions with a head diameter >0.5 μm or >2x the spine neck diameter; (2) stubby spines were dendritic protrusions with no discernable head and a length of ≤0.5 μm; and (3) thin/filopodia-like spines were dendritic protrusions with a length of >0.5 μm and head diameter <0.5 μm or no discernable head. During counting of dendritic spines, spine head diameters were also measured for analysis.

Statistics. All results are shown as mean ± s.e.m. All experiments were replicated in 3–16 rats. All data collection was randomized. All data were assumed to be normally distributed, but this was not formally tested. No statistical methods were used to predetermine sample sizes, but our sample sizes are similar to those reported in previous publications^{16–18}. All data were analyzed offline and investigators were blinded to experimental conditions during the analyses.

A total of 1,034 rats were used for this study, among which 394 were excluded from the final data analysis and interpretation due to the following reasons: (1) 67 rats were excluded because of health issues after surgeries (for example, >20% drop in body weight); (2) 272 were excluded because of the catheter failure, or failure in reaching the self-administration criteria; and (3) 55 were excluded due to off-target stereotoxic injections or poor viral expression.

Repeated experiments for the same group were pooled together for statistical analysis. Sample sizes were based on our previous studies performing similar experiments^{16,18,20}. For electrophysiology and dendritic spine experiments, the sample sizes are presented as n/m , where n is the number of cells and m is the number of rats. For behavioral experiments, the sample sizes are presented as n , which is the number of rats. Animal-based statistics were used for all data analyses, except for extracellular field excitatory postsynaptic potential (fEPSP) electrophysiology experiments, in which n is the number of recordings (Supplementary Fig. 4a). For electrophysiological experiments, we averaged the values of all the cells from each rat to obtain an animal-based mean value for statistical analysis^{16,18,20}. For dendritic spine experiments, we averaged individual dendritic segment values from each cell to obtain a cell-based value, and then averaged cell-based values from each rat to obtain animal-based values for statistical analysis^{60,61}. Statistical significance was assessed using unpaired *t*-tests, one-way analysis of variance (ANOVA) or repeated-measures two-way ANOVA, as specified in the related text. Two-tailed tests were performed for analyses. Statistical significance was set at $P < 0.05$ for all experiments. Statistical analyses were performed in GraphPad Prism (v.8). All of the main statistical results are presented in the main text, and additional statistical results are provided in Supplementary Table 1. Detailed experimental approaches, codes and reagents are presented in the Nature Research Reporting Summary section.

Reporting Summary. Further information on research design is available in the Nature Research Reporting Summary linked to this article.

Data availability

The data that support the findings of this study are available from the corresponding author upon request.

References

51. Mu, P. et al. Exposure to cocaine dynamically regulates the intrinsic membrane excitability of nucleus accumbens neurons. *J. Neurosci.* **30**, 3689–3699 (2010).
52. Brebner, K. et al. Nucleus accumbens long-term depression and the expression of behavioral sensitization. *Science* **310**, 1340–1343 (2005).
53. Mardilovich, K. et al. LIM kinase inhibitors disrupt mitotic microtubule organization and impair tumor cell proliferation. *Oncotarget* **6**, 38469–38486 (2015).
54. LaPlant, Q. et al. Dnmt3a regulates emotional behavior and spine plasticity in the nucleus accumbens. *Nat. Neurosci.* **13**, 1137–1143 (2010).
55. Maze, I. et al. Essential role of the histone methyltransferase G9a in cocaine-induced plasticity. *Science* **327**, 213–216 (2010).
56. Barrot, M. et al. CREB activity in the nucleus accumbens shell controls gating of behavioral responses to emotional stimuli. *Proc. Natl Acad. Sci. USA* **99**, 11435–11440 (2002).
57. Yu, J. et al. Nucleus accumbens feedforward inhibition circuit promotes cocaine self-administration. *Proc. Natl Acad. Sci. USA* **56**, 201707822 (2017).
58. Huang, Y. H., Schluter, O. M. & Dong, Y. Silent synapses speak up: updates of the neural rejuvenation hypothesis of drug addiction. *Neuroscientist* **21**, 451–459 (2015).
59. Winters, B. D. et al. Cannabinoid receptor 1-expressing neurons in the nucleus accumbens. *Proc. Natl Acad. Sci. USA* **109**, E2717–E2725 (2012).
60. Dumitriu, D., Rodriguez, A. & Morrison, J. H. High-throughput, detailed, cell-specific neuroanatomy of dendritic spines using microinjection and confocal microscopy. *Nat. Protoc.* **6**, 1391–1411 (2011).
61. Dumitriu, D. et al. Subregional, dendritic compartment, and spine subtype specificity in cocaine regulation of dendritic spines in the nucleus accumbens. *J. Neurosci.* **32**, 6957–6966 (2012).
62. Robinson, T. E. & Kolb, B. Alterations in the morphology of dendrites and dendritic spines in the nucleus accumbens and prefrontal cortex following repeated treatment with amphetamine or cocaine. *Eur. J. Neurosci.* **11**, 1598–1604 (1999).

Acknowledgements

We thank K. Tang and K. Churn for excellent technical support, as well as M. Varkey, M. Mulloth, S. Beriwal, S. Maddukkuri, Y. Jung, O. Ikwuegbu, R. Moazzam and A. Kang for assistance with behavioral training. This work was supported by NIH grant nos. NS007433 (W.J.W.), DA043940 (W.J.W.), DA023206 (Y.D.), DA044538 (Y.D.), DA040620 (Y.D., E.J.N.), DA047861 (Y.D.), DA035805 (Y.H.H.), MH101147 (Y.H.H.), DA008227 (E.J.N.) and DA014133 (E.J.N.); the NIDA Intramural Research Program (Y.S.); and a Mellon Fellowship (W.J.W.).

Author contributions

W.J.W., N.M.G., Y.H.H., Y.S., O.M.S., E.J.N. and Y.D. designed the experiments and analyses and wrote the manuscript. W.J.W., N.M.G. and P.A.N. performed electrophysiology experiments. W.J.W., N.M.G., L.F., A.S., N.M.-B. and K.I. performed behavioral training and testing. N.M.G. performed ELISAs. W.J.W. performed spine analysis, immunohistochemistry and confocal microscopy. P.J.H. and H.M.C. made the HSVs.

Competing interests

The authors declare no competing interests.

Additional information

Supplementary information is available for this paper at <https://doi.org/10.1038/s41593-019-0537-6>.

Correspondence and requests for materials should be addressed to Y.D.

Peer review information *Nature Neuroscience* thanks Rita A. Fuchs, Raphael Lamprecht and Manuel Mameli for their contribution to the peer review of this work.

Reprints and permissions information is available at www.nature.com/reprints.

Reporting Summary

Nature Research wishes to improve the reproducibility of the work that we publish. This form provides structure for consistency and transparency in reporting. For further information on Nature Research policies, see [Authors & Referees](#) and the [Editorial Policy Checklist](#).

Statistics

For all statistical analyses, confirm that the following items are present in the figure legend, table legend, main text, or Methods section.

n/a Confirmed

- The exact sample size (n) for each experimental group/condition, given as a discrete number and unit of measurement
- A statement on whether measurements were taken from distinct samples or whether the same sample was measured repeatedly
- The statistical test(s) used AND whether they are one- or two-sided
Only common tests should be described solely by name; describe more complex techniques in the Methods section.
- A description of all covariates tested
- A description of any assumptions or corrections, such as tests of normality and adjustment for multiple comparisons
- A full description of the statistical parameters including central tendency (e.g. means) or other basic estimates (e.g. regression coefficient) AND variation (e.g. standard deviation) or associated estimates of uncertainty (e.g. confidence intervals)
- For null hypothesis testing, the test statistic (e.g. F , t , r) with confidence intervals, effect sizes, degrees of freedom and P value noted
Give P values as exact values whenever suitable.
- For Bayesian analysis, information on the choice of priors and Markov chain Monte Carlo settings
- For hierarchical and complex designs, identification of the appropriate level for tests and full reporting of outcomes
- Estimates of effect sizes (e.g. Cohen's d , Pearson's r), indicating how they were calculated

Our web collection on [statistics for biologists](#) contains articles on many of the points above.

Software and code

Policy information about [availability of computer code](#)

Data collection

Electrophysiology data were recorded with Clampex 10.2 data acquisition software (Molecular devices, LLC). Behavioral data was collected with Med-PC software suite (Med Associates, Inc.). Microscopy data was collected with Leica Application Suite software (Leica Microsystems). ELISA absorbency measurements were collected with BioRad Microplate Manager Software (Bio-Rad Laboratories).

Data analysis

Electrophysiology data were analyzed with Clampfit 10 data analysis software (Molecular devices, LLC). Microscopy data was analyzed with Leica Application Suite software (Leica Microsystems) and Image J (NIH). Prism v7 (Graphpad Software) was used for all statistical analyses.

For manuscripts utilizing custom algorithms or software that are central to the research but not yet described in published literature, software must be made available to editors/reviewers. We strongly encourage code deposition in a community repository (e.g. GitHub). See the Nature Research [guidelines for submitting code & software](#) for further information.

Data

Policy information about [availability of data](#)

All manuscripts must include a [data availability statement](#). This statement should provide the following information, where applicable:

- Accession codes, unique identifiers, or web links for publicly available datasets
- A list of figures that have associated raw data
- A description of any restrictions on data availability

All data that support the findings presented in this study are available from corresponding authors upon reasonable request.

Field-specific reporting

Please select the one below that is the best fit for your research. If you are not sure, read the appropriate sections before making your selection.

Life sciences Behavioural & social sciences Ecological, evolutionary & environmental sciences

For a reference copy of the document with all sections, see nature.com/documents/nr-reporting-summary-flat.pdf

Life sciences study design

All studies must disclose on these points even when the disclosure is negative.

Sample size	No sample-size calculations were performed. All sample sizes used were based on our previous studies performing similar experiments (Lee et al., 2013; Ma et al., 2014; Graziane et al., 2016).
Data exclusions	Animals were excluded from further experimentation or data analysis if they displayed 1) catheter failure or failed to meet self-administration criteria (≥ 15 infusions/session, with 70% active to inactive nosepoke ratio on final training day); 2) misplaced stereotaxic injections or poor viral expression; and 3) health issues after surgery (e.g. 20% drop in body weight). For whole-cell electrophysiology, cells with $>20\%$ change in series resistance were excluded from data analysis. For minimal stimulation recordings, cells with $>15\%$ change in failure rates between rounds were excluded from data analysis.
Replication	All experiments were independently replicated in 3–16 rats, as reported within the figure. To verify reproducibility of the findings, many experiments were performed independently by separate investigators. In all cases findings were reproduced. Detailed methods are provided to replicate all experiments performed.
Randomization	For all experiments, animals were coded and randomly allocated to experimental and control groups.
Blinding	Investigators were blinded to experimental conditions during all analyses.

Reporting for specific materials, systems and methods

We require information from authors about some types of materials, experimental systems and methods used in many studies. Here, indicate whether each material, system or method listed is relevant to your study. If you are not sure if a list item applies to your research, read the appropriate section before selecting a response.

Materials & experimental systems		Methods	
n/a	Involved in the study	n/a	Involved in the study
<input type="checkbox"/>	<input checked="" type="checkbox"/> Antibodies	<input type="checkbox"/>	<input checked="" type="checkbox"/> ChIP-seq
<input type="checkbox"/>	<input checked="" type="checkbox"/> Eukaryotic cell lines	<input type="checkbox"/>	<input checked="" type="checkbox"/> Flow cytometry
<input type="checkbox"/>	<input checked="" type="checkbox"/> Palaeontology	<input type="checkbox"/>	<input checked="" type="checkbox"/> MRI-based neuroimaging
<input type="checkbox"/>	<input checked="" type="checkbox"/> Animals and other organisms		
<input type="checkbox"/>	<input checked="" type="checkbox"/> Human research participants		
<input type="checkbox"/>	<input checked="" type="checkbox"/> Clinical data		

Antibodies

Antibodies used	-Anti-GFP, mouse, monoclonal, Abcam, cat. no. ab1218, Lot no. GR213436-46, 1:1000 dilution -Anti-mouse, Alexa 488 conjugated, donkey, polyclonal, Abcam, cat. no. ab150105, Lot no. GR3249866-1, 1:500 dilution
Validation	The specificity of these antibodies have been validated by the manufacturer. Anti-GFP reactivity is invariant of species and recognized both wildtype and recombinant GFP, as well as under reduced and denatured conditions. It has been validated for ELISA, western blot, immunohistochemistry, and immunoprecipitation (https://www.abcam.com/gfp-antibody-9f9f9-ab1218.html). Anti-mouse is specific for mouse IgG. It has been validated for ELISA, Flow Cyt, and immunohistochemistry (https://www.abcam.com/donkey-mouse-igg-hl-alex-fluor-488-ab150105.html). Referenced are also included on the company webpages.

Eukaryotic cell lines

Policy information about cell lines	
Cell line source(s)	This study did not use cell lines.
Authentication	This study did not use cell lines.

Mycoplasma contamination

This study did not use cell lines.

Commonly misidentified lines
(See [ICLAC](#) register)

This study did not use cell lines.

Palaeontology

Specimen provenance

This study did not involve palaeontology.

Specimen deposition

This study did not involve palaeontology.

Dating methods

This study did not involve palaeontology.

Tick this box to confirm that the raw and calibrated dates are available in the paper or in Supplementary Information.

Animals and other organisms

Policy information about [studies involving animals](#); [ARRIVE guidelines](#) recommended for reporting animal research

Laboratory animals

All animals used in this study were male, Sprague-Dawley rats purchased from Charles River. Rats were ostnatal day 35-40 with 130-150 g body weight upon arrival. A total of 1034 rats were used for this study, among which 394 were excluded as detailed in the methods.

Wild animals

This study did not involve any wild animals

Field-collected samples

This study did not involve field collected samples.

Ethics oversight

All rats were used in accordance with protocols approved by the Institutional Care and Use Committees at the University of Pittsburgh and Icahn School of Medicine at Mount Sinai.

Note that full information on the approval of the study protocol must also be provided in the manuscript.

Human research participants

Policy information about [studies involving human research participants](#)

Population characteristics

This study did not involve human research participants.

Recruitment

This study did not involve human research participants.

Ethics oversight

This study did not involve human research participants.

Note that full information on the approval of the study protocol must also be provided in the manuscript.

Clinical data

Policy information about [clinical studies](#)

All manuscripts should comply with the ICMJE [guidelines for publication of clinical research](#) and a completed [CONSORT checklist](#) must be included with all submissions.

Clinical trial registration

This study did not use clinical data.

Study protocol

This study did not use clinical data.

Data collection

This study did not use clinical data.

Outcomes

This study did not use clinical data.

ChIP-seq

Data deposition

Confirm that both raw and final processed data have been deposited in a public database such as [GEO](#).

Confirm that you have deposited or provided access to graph files (e.g. BED files) for the called peaks.

Data access links

May remain private before publication.

This study did not use ChIP-seq.

Files in database submission

This study did not use ChIP-seq.

Genome browser session
(e.g. [UCSC](#))

This study did not use ChIP-seq.

Methodology

Replicates

This study did not use ChIP-seq.

Sequencing depth

This study did not use ChIP-seq.

Antibodies

This study did not use ChIP-seq.

Peak calling parameters

This study did not use ChIP-seq.

Data quality

This study did not use ChIP-seq.

Software

This study did not use ChIP-seq.

Flow Cytometry

Plots

Confirm that:

- The axis labels state the marker and fluorochrome used (e.g. CD4-FITC).
- The axis scales are clearly visible. Include numbers along axes only for bottom left plot of group (a 'group' is an analysis of identical markers).
- All plots are contour plots with outliers or pseudocolor plots.
- A numerical value for number of cells or percentage (with statistics) is provided.

Methodology

Sample preparation

This study did not use flow cytometry.

Instrument

This study did not use flow cytometry.

Software

This study did not use flow cytometry.

Cell population abundance

This study did not use flow cytometry.

Gating strategy

This study did not use flow cytometry.

Tick this box to confirm that a figure exemplifying the gating strategy is provided in the Supplementary Information.

Magnetic resonance imaging

Experimental design

Design type

This study did not use MRI.

Design specifications

This study did not use MRI.

Behavioral performance measures

This study did not use MRI.

Acquisition

Imaging type(s)

This study did not use MRI.

Field strength

This study did not use MRI.

Sequence & imaging parameters

This study did not use MRI.

Area of acquisition

This study did not use MRI.

Diffusion MRI

Used

Not used

Preprocessing

Preprocessing software

This study did not use MRI.

Normalization

This study did not use MRI.

Normalization template

This study did not use MRI.

Noise and artifact removal

This study did not use MRI.

Volume censoring

This study did not use MRI.

Statistical modeling & inference

Model type and settings

This study did not use MRI.

Effect(s) tested

This study did not use MRI.

Specify type of analysis: Whole brain ROI-based BothStatistic type for inference
(See [Eklund et al. 2016](#))

This study did not use MRI.

Correction

This study did not use MRI.

Models & analysis

n/a Involved in the study

- | | |
|--------------------------|-----------------------------------------------------------------------|
| <input type="checkbox"/> | <input type="checkbox"/> Functional and/or effective connectivity |
| <input type="checkbox"/> | <input type="checkbox"/> Graph analysis |
| <input type="checkbox"/> | <input type="checkbox"/> Multivariate modeling or predictive analysis |

Functional and/or effective connectivity

This study did not use MRI.

Graph analysis

This study did not use MRI.

Multivariate modeling and predictive analysis

This study did not use MRI.